DEPARTMENT OF PHYSICS
UNIVERSITY OF JYVÄSKYLÄ

The detection efficiency of the Clover Ge detector array at the RITU-GREAT facility

by
Anastasiia Girka

A thesis presented for the degree of
Master of Science

Supervisors: Professor Paul T. Greenlees;
Senior Researcher Catherine Scholey

Finland
May 2015

The detection efficiency of the Clover Ge detector array at the RITU-GREAT facility

Anastasiia Girka

Abstract

The absolute detection efficiency depending upon position along the beam direction is determined for three germanium detectors, that are part of the GREAT spectrometer at the focal plane of the RITU separator. The efficiency is determined for an energy range from 80 keV to 1400 keV for all three detectors as an array and also individually using digital electronics. The optimal position for the detector array has been defined for two configurations of the GREAT spectrometer: with the planar detector and without it. The obtained results have been compared with three references: a simulation prepared especially for this setup by another student using GEANT4, a previous study that was carried out by using analogue electronics and a simulation executed during the first years of the GREAT spectrometer's operation using GEANT3.

Contents

List of Figures

List of Tables

Introduction

The observation of radioactive decay products or nuclear reaction products and in particular γ-ray spectroscopy are ways in which experimental information can be obtained about nuclear processes. These experiments require detectors with reasonable efficiency and high energy resolution in order to extract the quantity and identity of γ-rays emitted from the nucleus of interest.

The most powerful detectors for γ-ray measurements are large volume High Purity Germanium detectors (HPGe) [1]. In the last few years a rapid progress in nuclear structure studies has been made thanks to the high quality data obtained with γ-ray spectroscopy experiments using large arrays such as EUROBALL [2], [3], GAMMASPHERE [4] and AGATA [5], based on HPGe detectors.

The exact knowledge of detection efficiency is important for discovering nuclear phenomena, as it is needed to determine transition intensities and consequently spin-parity and character of the transition observed. This thesis presents results of investigations of the absolute efficiency for an array of germanium detectors as a part of the GREAT spectrometer at the RITU separator focal plane for two assembles and the optimal position of the array. Before the present measurements only one similar study had been undertaken, but this was with analogue electronics, which is no longer used.

The aim of the present research was to make a comparison with the simulation, that is being developed for the current condition of the GREAT spectrometer in GEANT4 in parallel with these experiments. The RITU separator gives a distribution of ions at the focal plane, therefore the simulation needs to take this into account. Before using the simulation with the distributed source the accuracy has to be checked with the point source. Thus, comparison with experimental data is needed.

The experiments were carried out using three radioactive sources. The ^{133}Ba and ^{152}Eu sources have been used in order to cover an energy range from 80 keV to 1400 keV, with transition intensities that are well known. The energy range is wide enough to cover the range in which measurements are

usually taken. The ^{60}Co source has been used as a reference source, because it has a simple decay scheme with only two transitions. In addition, these radioactive sources have long half-lives, which is why they are commonly used in the nuclear physics laboratories.

This work is arranged in three chapters. Chapter 1 is devoted to

- the description of the RITU-GREAT set-up and germanium detectors utilized in it;
- the specifics of different experimental setups, which can be used for the cases of different assembles and location of the germanium detectors;
- the methods of processing the signals obtained from these detectors;
- the data acquisition system and determination of the absolute detection efficiency including determination of uncertainties.

The results of the present investigation are presented in Chapter 2. It contains an explanation how the results have been obtained, fitting coefficients and plots of absolute efficiency for the different assemblies and location of the germanium detectors. Chapter 3 is devoted to the discussion of the obtained results and comparison of the experiments and their simulations. The conclusions of the thesis concerning the prospects of utilization and further improvement of the GREAT clover detectors array are presented at the end of the paper.

Chapter 1

Theory and methods

1.1 The RITU gas-filled separator and the GREAT spectrometer

The RITU-GREAT set-up is a gas-filled recoil separator with a detection system located at its focal plane, which is utilized for experiments in the branch of nuclear physics at the Accelerator Laboratory of the University of Jyväskylä, Finland. The separator name means Recoil Ion Transport Unit. Generally speaking, an in-flight separator is used to select reaction products recoiling out of a thin target from primary beam by using a magnetic field [6]. RITU is located after a target chamber. The main feature of it as a gas-filled separator is the average charge state of the products at the focal plane (Fig. 1.1, [6]), because ions passing through its magnets, the chamber of which is filled with a helium gas, undergo many charge changing collisions. This leads to a decrease in image size at the focal plane, thus the transmission of the separator becomes higher [7].

The detection system at the focal plane of the separator is an integral part of the facility, since the separated particles need to be detected. The RITU separator has the GREAT spectrometer as a detection system, which was developed as a collaboration project between the Nuclear Physics Group at STFC Daresbury Laboratory, and the nuclear physics groups at the Universities of Liverpool, Manchester, Surrey, York and Keele within the United Kingdom [8] and JYFL, Finland. The name of the system is an abbreviation from the words gamma, recoil, electron, alpha and timing in a sense that mentioned particles can be detected with a negligibly small dead time, because of the triggerless data acquisition system (DAQ). The focal plane detection system consists of the following parts (Fig. 1.2, [9] and Fig. 1.3, [10]):

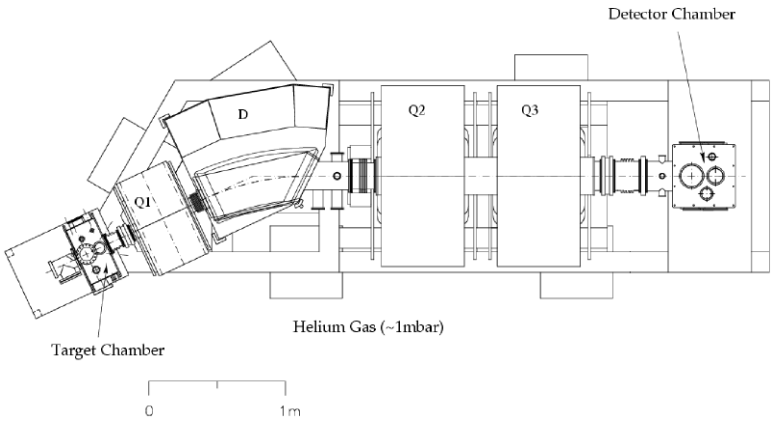

Figure 1.1: The scheme of the RITU gas-filled recoil separator. Q1, Q2 and Q3 are quadruples for focusing and D is a dipole for bending particles.

1. A high efficiency *segmented germanium clover detector* (Top Clover) and *two side high-purity germanium clover detectors* (FPClover01 and FPClover02) to measure the energies of higher energy γ-rays and a *double-sided planar germanium strip detector* (Planar detector) to measure the energies of X-rays, low energy γ-rays and beta-particles;

2. *A multiwire proportional counter* (MWPC) filled with isobutane, which acts as an active recoil discriminator, here the energy-loss and position of recoils are recorded;

3. An array of 28 *silicon PIN photodiode detectors* to measure conversion electron energies and escaping alpha-particles;

4. *Double sided silicon strip detector* (DSSSD) consisting of two adjacent parts, into which the reaction products are implanted, it is utilized to measure alpha-particles, beta-particles, proton emission or conversion electrons;

5. *Total data readout* (TDR) system, which is a triggerless system, it was created in order to decrease the deadtime of the DAQ.

Figure 1.3 shows the relative position of these detectors.

The detectors for γ-ray spectroscopy must have enough depletion depth and active volume to be able to detect such penetrative radiation as γ-rays. For this reason the technique for reducing impurity concentration in the germanium crystals was developed.

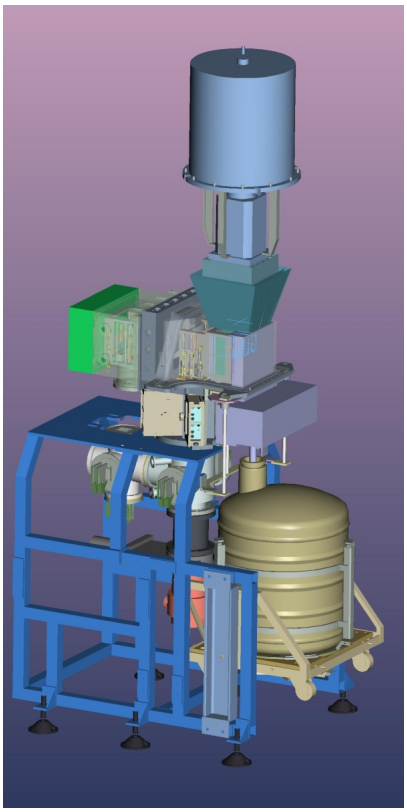

Figure 1.2: General view of the GREAT spectrometer.

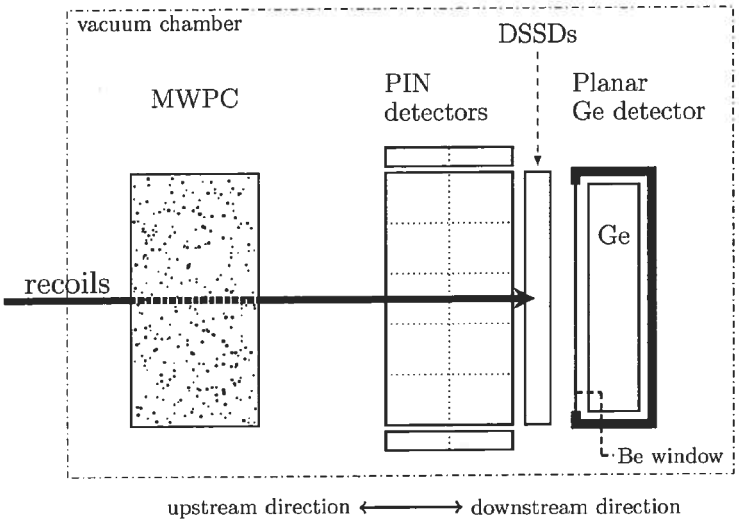

Figure 1.3: Relative positions of the detectors at the GREAT spectrometer.

Detectors with these ultra-pure germanium crystals are called high purity germanium detectors (HPGe-detectors). These germanium detectors are often surrounded by bismuth germanate (BGO, $Bi_4Ge_3O_{12}$) scintillation detectors, which act as a shield in order to detect and reject the Compton scattered γ-rays from the germanium crystal.

The Top Clover detector is a high efficiency germanium detector. It is made from 4 germanium crystals (which is why it is called clover detector) packed in a common cryostat, but the outer surface of the individual crystals can be electronically segmented into 4 regions, so that the detector would has 16 segments in all (Fig. 1.4, [11]). The segmentation is a typical solution to increase the efficiency of the detector by reducing the counting rate in each channel and reducing pile-up. In the first years of the GREAT operation this detector was installed behind the planar detector (behind detector chamber), thus it was possible to associate spatially each segment with a decay process occurring in the planar detector. But nowadays this clover detector is located on the top of detector chamber. The initial dimensions of crystals were 70 mm in diameter and 90 mm long, but then they have been shaped to match the geometry of the focal plane. The present dimensions are as follows: the non-tapered square is 45.5 mm per side, the length of the tapered part is 36 mm and the tapered end is a square with 41 mm per side.

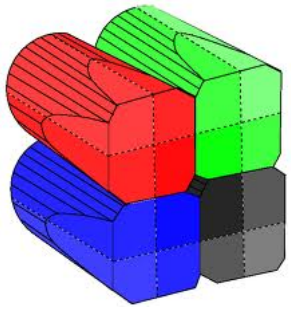

Figure 1.4: The 16 segments of the Top Clover detector.

Two side high-purity germanium clover detectors, FPClover01 and FPClover02 consist of 4 crystals each and they are not segmented. They are smaller than the Top Clover detector [12] and are located on the sides of detector chamber, along the y-axis (Fig. 1.5). Their total length is 105 mm, the non-tapered square is 61.5 mm per side, the length of the tapered part is 30 mm and the tapered end is a square with 54 mm per side.

The planar germanium detector contains a pure germanium crystal with dimensions $\sim$ 12 cm $\times$ 6 cm and thickness 15 mm. It has a beryllium entrance window to decrease the absorption for low-energy γ-rays ($\sim$ 10 keV

- 200 keV), the window thickness is 0.5 mm. The thickness of the aluminum shell is 3 mm, but the rear side has a 1 mm window facing the Ge area. The planar detector is segmented with 24 vertical strips on the side of beryllium window and 12 horizontal strips on the other side. This segmentation allows one to determine the coordinates of an incoming γ-ray, thus this detector is position sensitive. The segmentation of the detector also gives the possibility to make a γ-γ coincidence analysis using only the planar detector.

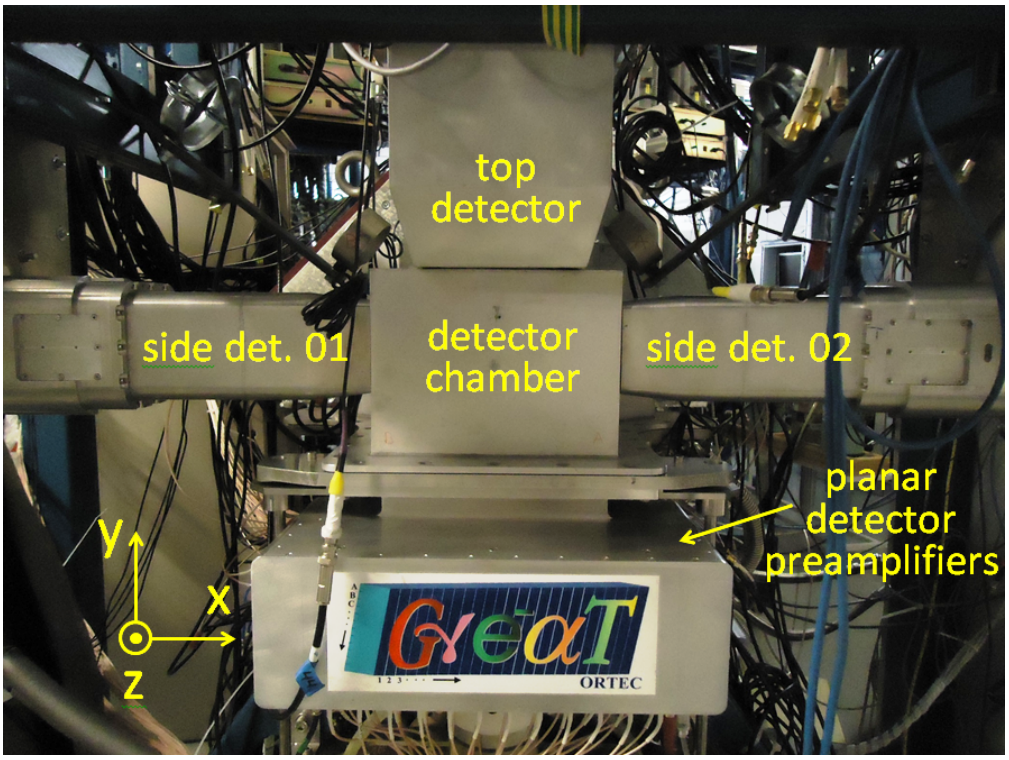

Figure 1.5: Location of the clovers relative to the GREAT detector chamber. View against the beam direction. The planar detector is inside the detector chamber. The z-direction goes out from the page.

1.2 Experimental setup

In the present work an array of focal plane germanium detectors have been investigated: Top Clover, FPClover01, FPClover02 and planar detector. A photograph of the setup with both side and Top Clover detectors are presented in Fig. 1.5. The axes are designated in a traditional way: a vertical axis is y-axis, a transverse horizontal one is the x-axis and an axis

along which the beam is coming to the detector chamber is the z-axis. The two side detectors (FPClover 01 and FPClover 02) are located along x-axis facing each other, on either side of the detector chamber and they are about 2 times smaller than the Top Clover detector. The Top Clover is located along the y-axis, directly above the detector chamber. The planar detector is placed inside the detector chamber, it is the last detector in the beam direction, before it are the DSSD detectors, in which the recoiling nuclei are implanting.

The Top Clover and side clovers are fixed on a movable framework, so that one can slide the frame and change the position of the detectors along the z-axis. The position is important because of the contents of the detector chamber and also for access to the chamber: a multiwire proportional counter, silicon PIN photodiode detectors, silicon DSSD detectors and germanium planar detector (in order downstream the beam). On the top bar of the movable frame there is a position indicator, which includes a ruler and pointer, the ruler counts in the upstream beam direction (Fig. 1.6, [13]). In the previous investigation with analogue electronics the position of 105 mm (according to the indicator) was determined as the optimal one, this position was measured from the end of the top bar, so the absolute value of it is 1714 mm [13]. In the present investigation we have utilized digital electronics (including the TDR system), which are now becoming more commonly used in the Nuclear spectroscopy research group set-ups (RITU, GREAT, JUROGAM II, etc.).

For the performed measurements point sources were used (Table 1.1) and placed in the centre of the DSSDs empty printed circuit board (PCB) is in the Fig. 1.7. Each source was used separately. The reasons for using the point source were to obtain the experimental data without any special features, that can appear using the distributed source, and to make a comparison of the experimental data obtained using the point source with the simulation data, because the accuracy of the simulation has to be proven with data from the point source first before making a simulation for the distributed source.

Code	**Element**	**Calibration date**	**Calibrated activity**, [kBq]
JYFL-82	^{133}Ba	01.04.03	42.4 ($\pm$ 3%)
JYFL-81	^{152}Eu	01.04.03	40.1 ($\pm$ 3%)
JYFL-80	^{60}Co	01.04.03	401 ($\pm$ 3%)

Table 1.1: List of the sources used.

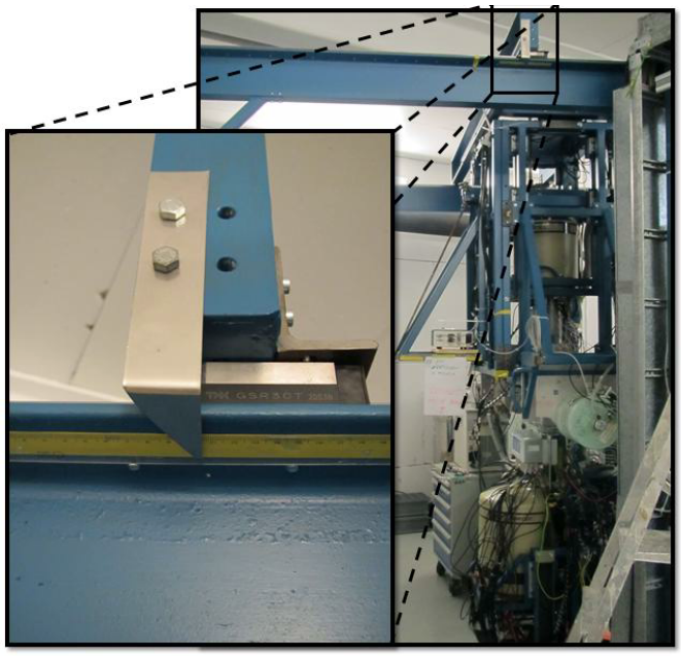

Figure 1.6: The position indicator at the top bar of the movable frame [13].

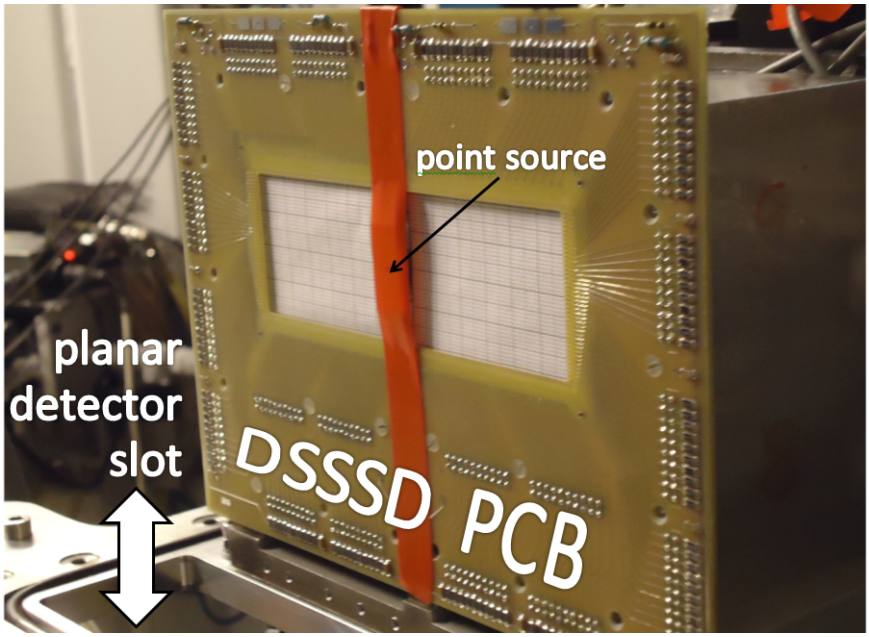

Figure 1.7: The point source location on the DSSSD PCB.
The slot for the planar detector is visible in front of DSSSD PCB.

The duration of each measurement was 1 hour 30 minutes, which was long enough to collect sufficient statistics, that the peak fitting could be done with a low uncertainty. Two sets of measurements were performed: with the planar detector in place (inside the detector chamber) and without the planar detector (it was removed from the detector chamber). This operation is relatively easily to do, because under the detector with its LN_2 dewar there is a jack-screw, which is intended for moving the planar detector up and down. The operation of removing the detector has been carried out to verify the absorption effects it has on the γ-rays that then enter the Clover detectors. This can be reproduced in the simulations if the detector geometries and materials are correct. Thus there are two alternative goals of the experiments: to check the attenuation of the γ-rays due to the planar detector and verify the most efficient position of the Clover detectors with and without the planar detector. For each source 3 measurements were made with different positions of the framework: 95 mm, 105 mm, 115 mm. These values were chosen based on the previous research, when the position of 105 mm was determined as optimal [13].

In summary each set of measurements consists of 9 measurements. The data analysis has also been made by applying the so-called add-back algorithm (see next section). All together 144 energy spectra have been obtained in order to fit the full-energy peaks and plot the efficiency curves.

1.3 Signal processing and data acquisition

Germanium detectors are semiconductor detectors, which are intended for the detection of ionizing radiation. The detector works as a semiconductor diode. Therefore it applies the principle of a p-n junction: when a γ-ray enters to the depletion region of a crystal, it creates electron-hole pairs in an amount, which is proportional the energy of the γ-ray. Then the electrons are attracted to the p-type region and holes are attracted to the n-type region (Fig. 1.8). The contact potential of p-n junction is about a few keV, it is applied to the crystal for collecting the charge, that was created by a γ-ray. As a result of this outer action the electrical impulse is created in the outside circuit of the detector and are amplified afterward.

The detectors for γ-ray spectroscopy must have enough depletion depth or active volume to be applicable for detecting such penetrative radiation as γ-rays. For this reason the technique for reducing impurity concentration in germanium crystals was developed in the mid-1970s ([14]). Detectors with these ultrapure germanium crystals are called high-purity germanium detectors (HPGe-detectors), they operate as fully depleted detectors with

bias voltages of a few thousand volts.

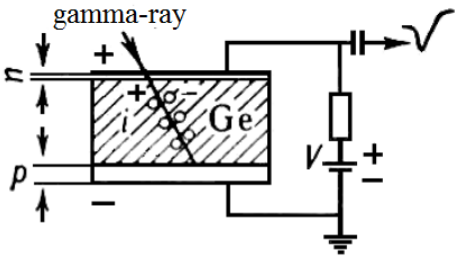

Figure 1.8: The operational scheme of the semiconductor germanium detector.

At the beginning of the signal processing the γ-ray produces an impulse, the magnitude of which is proportional the energy of the γ-ray, then this pulse goes through the preamplifier which is built-in into the detector. The electronics scheme for the germanium detectors at the GREAT spectrometer is shown in the Figure 1.9, where abbreviations "FPGe" are applied to indicate the side clovers. There is one signal that carrying energy information from each germanium crystal or segment and one logic signal from the BGO-shield (this is not shown on the scheme for simplicity) that contains information on the Compton scattering from the Ge-detector.

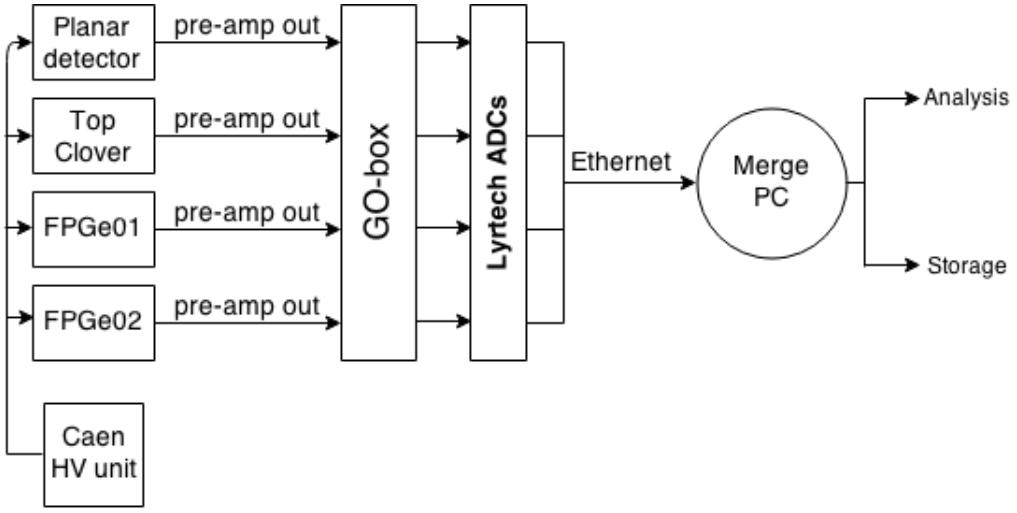

Figure 1.9: The scheme of electronics used with germanium detectors at the GREAT spectrometer.

The digitized signals from the crystals are handled by the triggerless

total data readout (TDR) system [15]. The triggerless TDR system is an improvement of previous systems due to the absence of common hardware trigger, as it allows one to process the data from each channel independently without losses caused by a common trigger read out dead time. For many years this system was unique. It includes a 100 MHz clock, which provides time-stamping for the data items with 10 ns precision and synchronization pulses to all ADCs. Data items are then arranged into a single time-ordered stream of data in collate and merge software. The merge PC on the scheme (Fig. 1.9) is a personal computer with MIDAS software installed [16]. By the aid of this software the merging of signals from all channels is performed along with the writing of spectra are done. There is also a possibility to see spectra during the running of an experiment using MIDAS.

Furthermore, there is a possibility to analyze spectra online with the Grain software [17] and this is a remarkable feature of the JYFL facilities. Grain is used for both online and offline sorting of the data, for visualization of spectra and primary analysis. The sorting procedure means selecting events from the stream of data to build the spectra, in the simplest case there are spectra for each detector or crystal individually. It is a very flexible tool, since it is a Java code (Appendix A) that is written for every single case, that allows the user to impose conditions of time and energy values for every event and also have some spatial analysis if position sensitive detectors are involved in the experiment.

Another undisputed advantage of using the sorting procedure is the possibility to make so-called add-back processing of the data from clover detectors. The add-back algorithm is designed to recover Compton-scattered γ-rays in cases where the scattered γ-ray is absorbed in another crystal, not escaped from it. Add-back is made by setting a time window for neighboring crystals in the clover detector. Therefore if there are signals during the window-time then the impulses are treated as a single event and their energies will be added. This feature of the sorting procedure allows one to get the best results from a composite detector.

After sorting of the obtained γ-ray spectra an energy calibration must be performed. The pulse height scale on the spectrum must be calibrated in terms of absolute γ-ray energy to identify γ-rays of unknown energy in the next experiments or to determine energy resolution of the detector defined by the Full Width at Half Maximum (FWHM) of the peak. It is better to have several calibration peaks along the measured energy range, because non-linearities can occur among all utilized channels.

Each crystal corresponds to one electronics channel and every channel has to be calibrated. The energy calibration procedure includes a review of at least 6 peaks in the spectrum from low to high energy. The centroids of

the chosen peaks are fitted with a Gaussian distribution function simultaneously using the Grain software. This procedure allows one to obtain three calibration coefficients that describe the energy of the peaks at a particular channel by a quadratic equation: $E_\gamma = a \cdot x^2 + b \cdot x + c$, where x is the spectrum channel number. All the coefficients are stored in a separate file with extension "*.gains". When the calibration coefficients for a certain channel are put into the file, the calibration can be checked by sorting and overlaying the spectra from the 4 crystals, which correspond to one detector, in order to see that they match to each other. If one source is not sufficient for a good calibration, one can sort the data from two or more radioactive sources to one spectrum and thus use more peaks for calibration.

The energy spectra collected with the full array of Ge-detectors (at relative position of 105 mm, without the planar detector) are presented in Figures 1.10 - 1.12 with ^{133}Ba, ^{152}Eu and ^{60}Co sources correspondingly. The spectra are typical for HPGe-detectors with their high energy resolution. On the ^{133}Ba spectrum (Fig. 1.10) one can see a lot of x-rays and Compton scattering events for energies starting from 25 keV to 276 keV. This may cost falsely result of the peak fitting procedure especially for such small peaks as at 160.613 keV and 223.234 keV, thus the background subtraction routine is needed and it was applied in the present research.

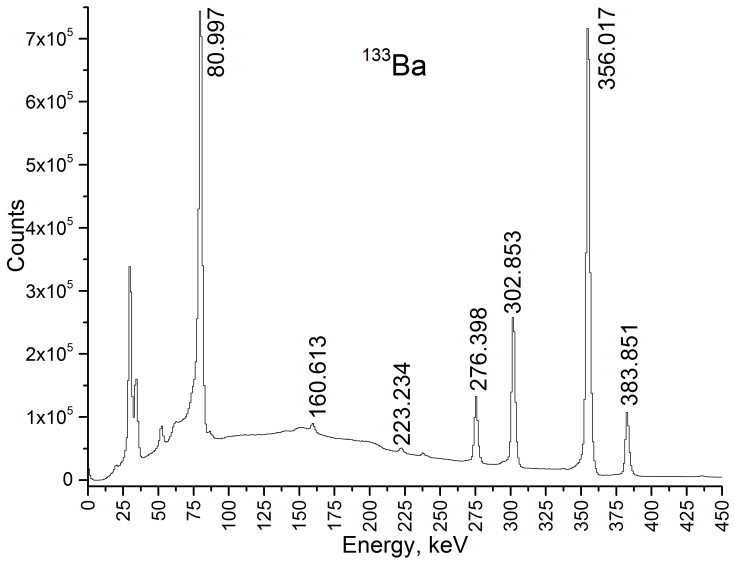

Figure 1.10: ^{133}Ba spectrum collected with the full array of Ge-detectors.

There is also a lot of x-rays events registered on the ^{152}Eu spectrum in the range of low energies, but the γ-ray transitions in that region have high enough intensities. However, for small peak at 688.675 keV the background

subtraction is required for reliable fitting results. On the ^{60}Co spectrum one can see not only full energy peaks (1173.2 keV and 1332.5 keV), but also so-called Compton spectrum at the lower energies. The Compton spectrum consists of events, in which the γ-ray underwent Compton scattering, escaped from the Ge-crystal and its full energy was not registered by the detector.

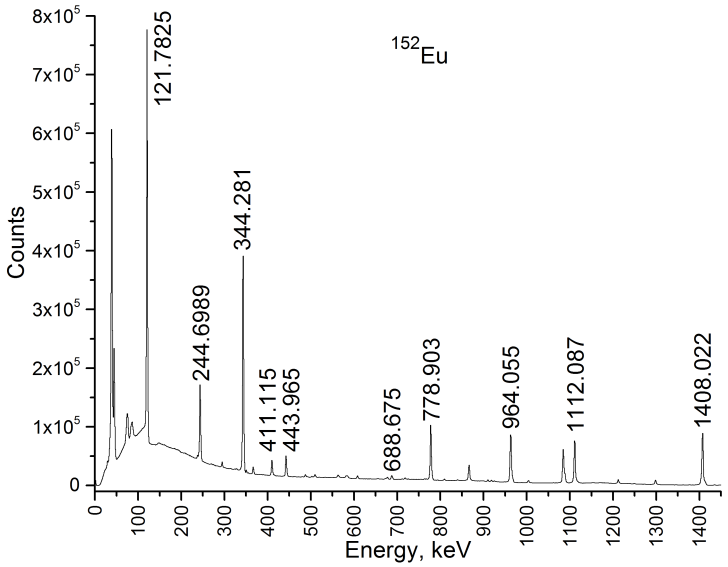

Figure 1.11: ^{152}Eu spectrum collected with the full array of Ge-detectors.

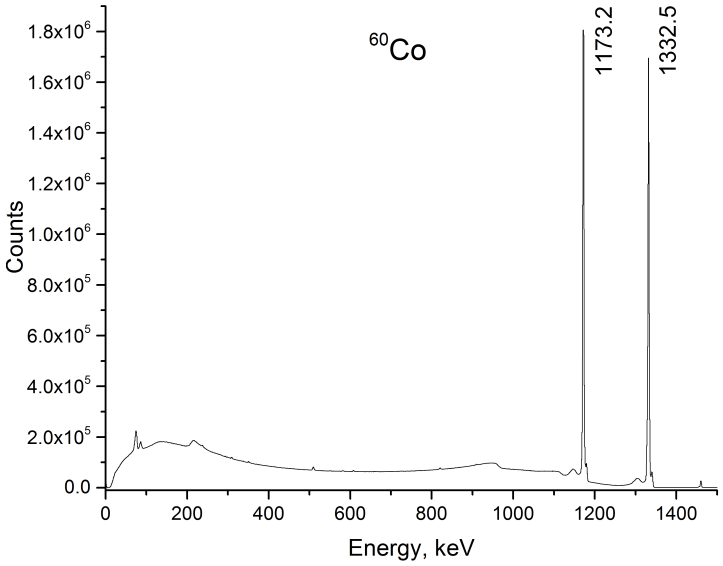

Figure 1.12: ^{60}Co spectrum collected with the full array of Ge-detectors.

1.4 Determination of the detection efficiency

An absolute photopeak efficiency is the number of γ-rays recorded by the detector and data acquisition system divided by the number of γ-rays emitted by the source [18]:

$$\varepsilon_{abs} = \frac{N_{FEP}}{N(E)} \cdot 100[\%], \tag{1.1}$$

where N_{FEP} is the number of full energy photopeak γ-rays and it means the number of recorded γ-ray of a certain energy and $N(E)$ is the number of emitted γ-rays of a certain energy.

The number of emitted γ-rays $N(E)$ is the number of decays occurred during an experiment N_{tot} multiplied by relative intensity $I_\gamma(E)$ (see Tables 1.2-1.4, [19]) for a certain energy:

$$N(E) = N_{tot} \cdot I_\gamma(E). \tag{1.2}$$

Barium		
Energy, keV	**Intensity**	**Error**
80.997	340.6	2.7
160.613	6.45	0.08
223.234	4.50	0.04
276.398	71.64	0.22
302.853	183.3	0.6
356.017	620.5	1.9
383.851	89.4	0.3

Table 1.2: The relative intensities of γ-ray transitions in ^{133}Cs with errors from a closed ^{133}Ba source (normalized to 1000 decays).

In turn, the number of decays N_{tot} is defined as

$$N_{tot} = A_{source} \cdot \Delta t, \tag{1.3}$$

where Δt is the duration of a measurement. The value A_{source} in equation 1.3 is the activity of the source at the time of measurement. Usually, the activity of the source is given by manufacturer for the day of calibration,

Europium		
Energy, keV	**Intensity**	**Error**
121.7825	286.5	1.3
244.6989	75.82	0.46
344.281	266.0	1.2
411.115	22.62	0.13
443.965	31.25	0.19
688.675	8.80	0.08
778.903	130.17	0.44
964.055	147.58	0.44
1112.087	135.81	0.48
1408.022	209.45	0.59

Table 1.3: The relative intensities and errors for the closed ^{152}Eu source (normalized to 1000 decays).

Cobalt		
Energy, keV	**Intensity**	**Error**
1173.2	99.89	0.02
1332.5	99.9810	0.0015

Table 1.4: The relative intensities and errors for the closed ^{60}Co source (normalized to 100 decays).

then one should recalculate the value for the certain day taking into account the half-life of the source $T_{1/2}$ and time passed from the day of calibration t:

$$A_{source} = A_{calib} \cdot e^{\frac{ln2}{T_{1/2}} \cdot t} \tag{1.4}$$

The uncertainties for the values from the equations (1.1-1.4) were estimated as a systematical error. Thus, for the absolute efficiency the equation for the uncertainty is as follows:

$$\delta\varepsilon_{abs} = \left|\frac{\partial\varepsilon_{abs}(N_{FEP}, N(E))}{\partial N_{FEP}} \cdot \delta N_{FEP}\right| + \left|\frac{\partial\varepsilon_{abs}(N_{FEP}, N(E))}{\partial N(E)} \cdot \delta N(E)\right| + \varepsilon_{abs} \cdot \frac{\delta A_{calib}}{A_{calib}} = \frac{\delta N_{FEP}}{N(E)} + \frac{\delta N(E) \cdot N_{FEP}}{N(E)^2} + \varepsilon_{abs} \cdot \frac{\delta A_{calib}}{A_{calib}}, \tag{1.5}$$

then for number of emitted γ-rays of a certain energy:

$$\delta N(E) = \Big|\frac{\partial N(E)(N_{tot}, I_\gamma(E))}{\partial N_{tot}} \cdot \delta N_{tot}\Big| + \Big|\frac{\partial N(E)(N_{tot}, I_\gamma(E))}{\partial I_\gamma(E)} \cdot \delta I_\gamma(E)\Big| = I_\gamma(E) \cdot \delta N_{tot} + N_{tot} \cdot \delta I_\gamma(E). \tag{1.6}$$

For the total number of decays N_{tot} the uncertainty was calculated by this equation:

$$\delta N_{tot} = \Big|\frac{\partial N_{tot}(A_{source}, \Delta t)}{\partial A_{source}} \cdot \delta A_{source}\Big| + \Big|\frac{\partial N_{tot}(A_{source}, \Delta t)}{\partial \Delta t} \cdot \delta \Delta t\Big| = \Delta t \cdot \delta A_{source} + A_{source} \cdot \delta \Delta t, \tag{1.7}$$

where δA_{source} was calculated in the following way using the value of δA_{calib}, which is 3% from the value A_{calib} (1.1):

$$\begin{aligned} \delta A_{source} = &\Big|\frac{\partial A_{source}(A_{calib}, F(t, T_{1/2}))}{\partial A_{calib}} \cdot \delta A_{calib}\Big| + \\ &\Big|\frac{\partial A_{source}(A_{calib}, F(t, T_{1/2}))}{\partial F(t, T_{1/2})} \cdot \delta F(t, T_{1/2})\Big| = \\ &F(t, T_{1/2}) \cdot \delta A_{calib} + A_{calib} \cdot \delta F(t, T_{1/2}) \end{aligned} \tag{1.8}$$

In equation (1.8) $F(t, T_{1/2})$ is denoted for the $e^{-\frac{ln2}{T_{1/2}} \cdot t}$, since it is a complex function and uncertainty for it should be calculated separately:

$$e^{-\frac{ln2}{T_{1/2}} \cdot t} = F(t, T_{1/2}), \tag{1.9}$$

$$\begin{aligned} \delta F(t, T_{1/2}) = &\Big|\frac{\partial F(t, T_{1/2})}{\partial t} \cdot \delta t\Big| + \Big|\frac{\partial F(t, T_{1/2})}{\partial T_{1/2}} \cdot \delta T_{1/2}\Big| = \\ &\Big|-\frac{ln2}{T_{1/2}} \cdot e^{-\frac{ln2}{T_{1/2}} \cdot t} \cdot \delta t\Big| + \Big|ln2 \cdot t \cdot e^{-\frac{ln2}{T_{1/2}} \cdot t} \cdot T_{1/2}^{-2} \cdot \delta T_{1/2}\Big|. \end{aligned} \tag{1.10}$$

The error for time passed from the day of calibration Δt was taken as unit, since measurements were done in one day or in the evening of one day and in the morning of the next day, in any case within twenty-four hours.

The values of half-lives $T_{1/2}$ were taken from the data-sheet provided by manufacturer (see Table 1.5, [20]).

Code	**Element**	$T_{1/2}$, days
JYFL-82	^{133}Ba	3848 ± 6
JYFL-81	^{152}Eu	4943 ± 5
JYFL-80	^{60}Co	1925.3 ± 0.4

Table 1.5: The half-lives of the source nuclides, that were used in the experiment, according the manufacturer data.

The duration of each measurement was one hour and a half as stated in section 1.2, the error value was taken to be 5 min.

The number of recorded γ-rays of a given energy N_{FEP} (Eq. 1.1) is the area of the peak in the spectrum, which is approximately Gaussian. The Radware software package [21] was used for the peak fitting and area analysis. It was designed for γ-ray spectroscopy and has good fitting and background subtraction routines.

Chapter 2

Results

The 48 plots obtained from experimental data of absolute efficiency required fitting. As it was done in the previous research ([13]) and proposed by S. Hurtado and others ([22]) for the region 36-1500 keV the following function was fitted to the data:

$$\varepsilon = A(e^{-B \cdot X^C} + e^{-D \cdot X^E})(1 - e^{F \cdot X^G}), \tag{2.1}$$

where X is the energy of the gamma-ray and A, B, C, D, E, F and G are the fitting parameters, the initial values for which were proposed ([22]) as follows: 3.16, 0.049, 0.729, 0.753, 0.219, -0.011 and 0.92. For these studies the Origin scientific graphing and data analysis software ([23]), namely OriginPro 9, and its tool Nonlinear Curve Fit was used.

The ^{133}Ba and ^{152}Eu sources were used to obtain a whole range of energies. The ^{60}Co source was used for absolute efficiency measurements. The ^{152}Eu and ^{133}Ba data were normalized to the ^{60}Co 1332 keV photopeak efficiency. A normalization factor of 0.9 ± 0.1 was obtained. The ^{60}Co source is taken as a reference, because its decay scheme is very simple: it has only two transitions with a relative intensity close to 100%.

For the set of measurements with planar detector the optimal position was 115 mm (Fig. 2.2), whereas the optimal position of the Clover detectors without planar detector it was 95 mm (Fig. 2.3). The efficiency curves for each detector individually for all 3 positions are presented in Appendix B for the configuration with the planar detector installed and in Appendix C for the case, when the planar detector was removed. By applying the add-back algorithm, more differences between the efficiency curves can be observed (Fig. 2.4 and 2.5). The results of determination of the total efficiency are presented in graphical form, because it is convenient for visual comparison of the curves obtained by different methods. In each plot (Fig. 2.6- Fig. 2.13) there are two curves, one is related to the sorting that has been done

by applying an add-back method and another one related to the case when add-back was not applied. As it is expected, the case of applying add-back shows better absolute efficiency in the region of higher energy, while in the region of lower energies there is almost no difference between these curves. This is because for γ-rays of low energies ($<$200 keV in germanium) the dominant interaction phenomenon with matter is photoelectric effect (Fig. 2.1), but add-back algorithm is designed to recover Compton scattered γ-rays. Another observation is that the absolute efficiency is lower when the planar detector is inside the detector chamber; this is observable for all three detectors as an array as well as for each detector individually.

Plots 2.6- 2.9 are related to the set of measurements with the planar detector installed, starting from the plot for the array of the detectors (Fig. 2.6), then for the Top Clover (Fig. 2.7) and for side clovers (Fig. 2.8 and Fig. 2.9). The next four plots (Fig. 2.10- 2.13) present the results of the set of measurements without planar detector, they are in the same order as before: the plot for the array (Fig. 2.10), then the plot for the side clovers (Fig. 2.13).

The coefficients of the fitting equation (Eq. 2.1) for the presented curves are in the tables 2.1 - 2.4, the last row in each table corresponds to the correlation coefficient R^2, whose value should be close to 1 when the fit is perfect. According to the obtained values, all the fits are very good.

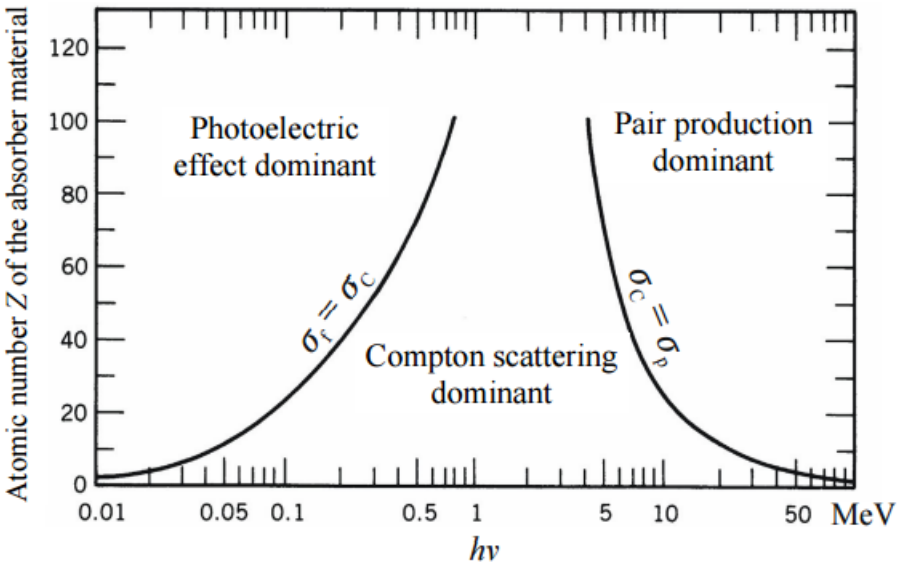

Figure 2.1: Interaction of gamma radiation with matter.

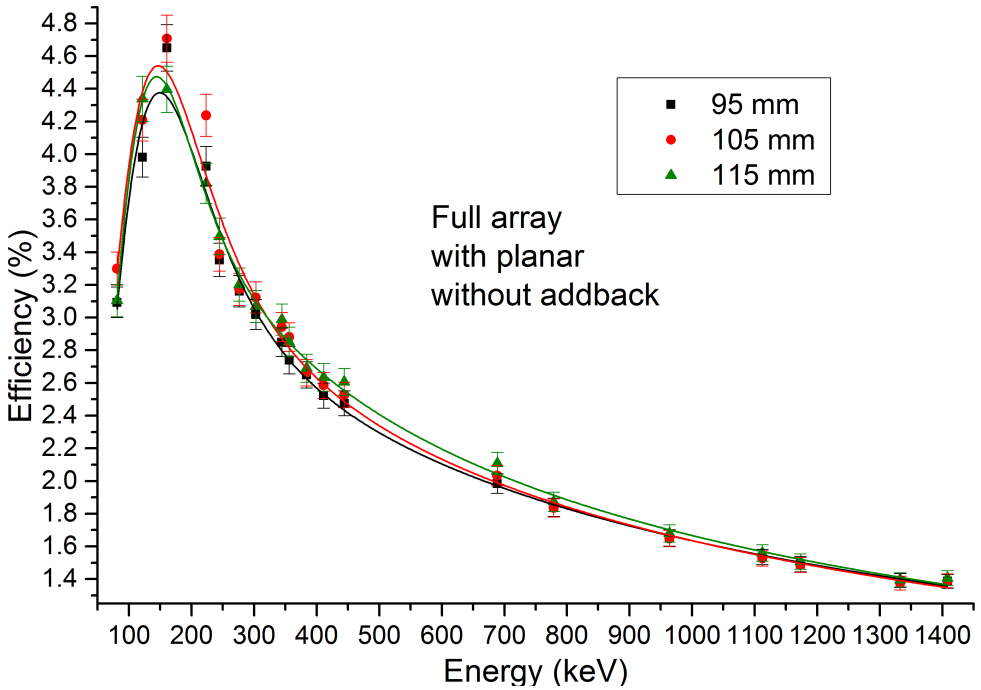

Figure 2.2: Absolute efficiency curves for the array of 3 clover detectors and for all 3 positions (95 mm, 105 mm, 115 mm) without application of an add-back algorithm, the setup is equipped with planar detector.

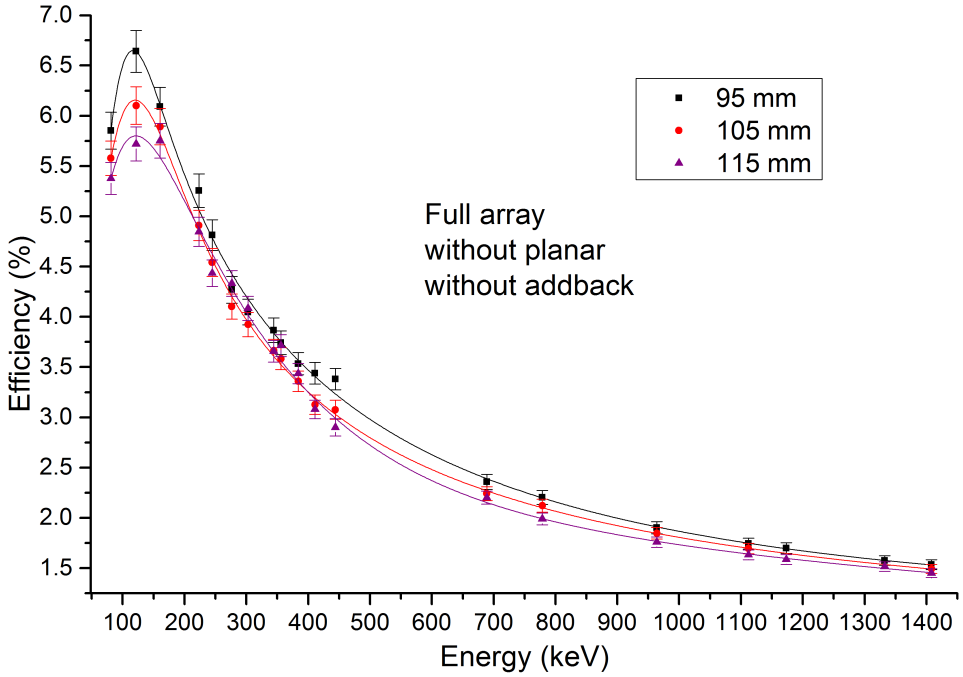

Figure 2.3: Absolute efficiency curves for the array of 3 clover detectors and for all 3 positions (95 mm, 105 mm, 115 mm) without application of an add-back algorithm, the planar detector is removed.

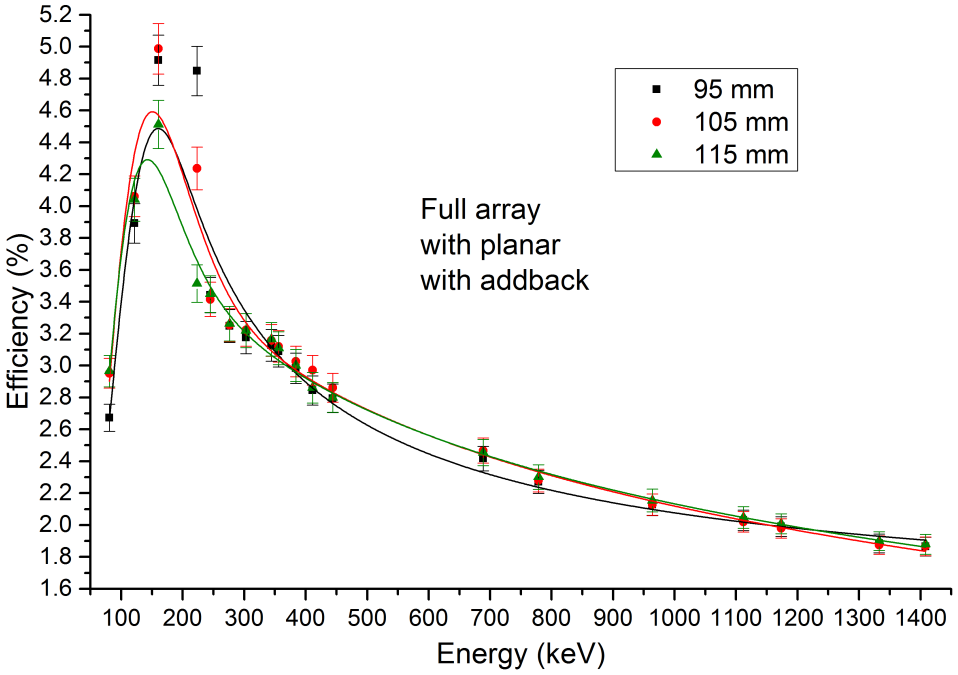

Figure 2.4: Absolute efficiency for the array of 3 clover detectors and for all 3 positions (95 mm, 105 mm, 115 mm) applying the add-back algorithm, the setup is equipped with planar detector.

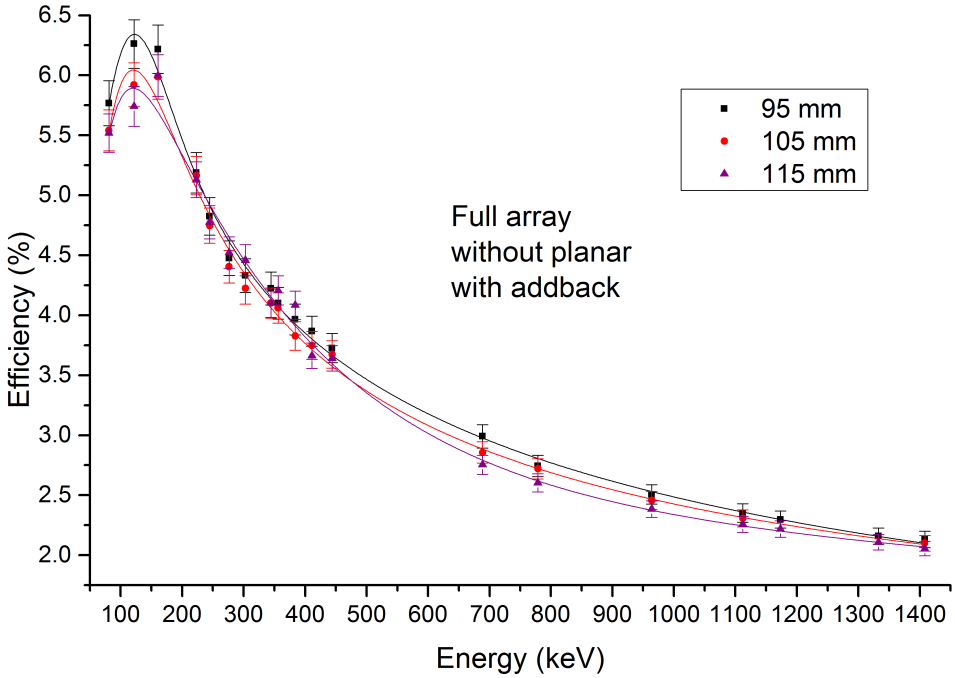

Figure 2.5: Absolute efficiency for the array of 3 clover detectors and for all 3 positions (95 mm, 105 mm, 115 mm) applying the add-back algorithm, the planar detector is removed.

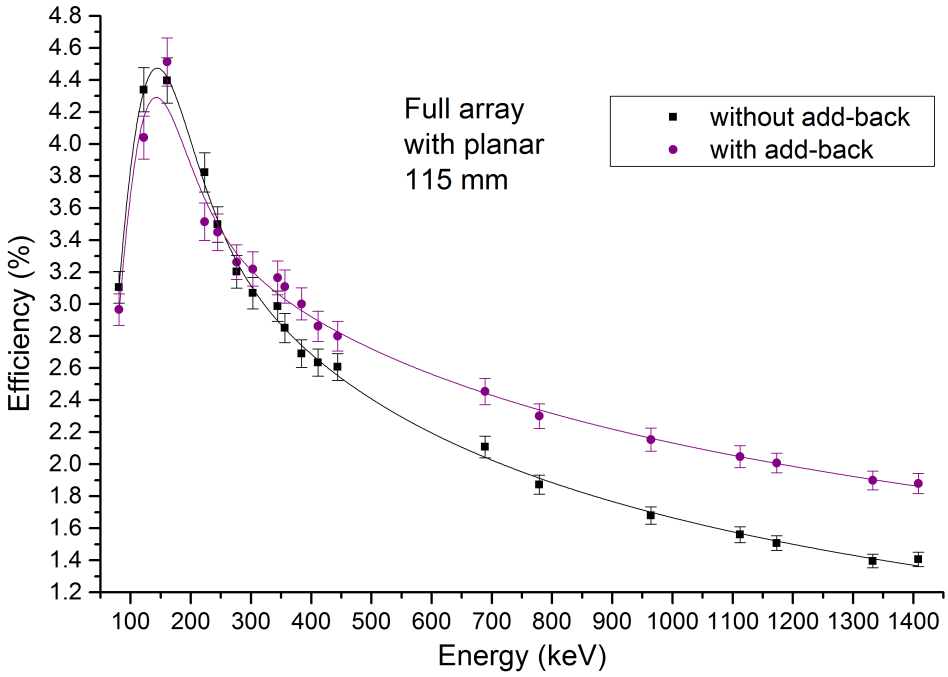

Figure 2.6: Absolute efficiency for the array of 3 clover detectors. The relative position of the frame is 115 mm, the setup is equipped with planar detector.

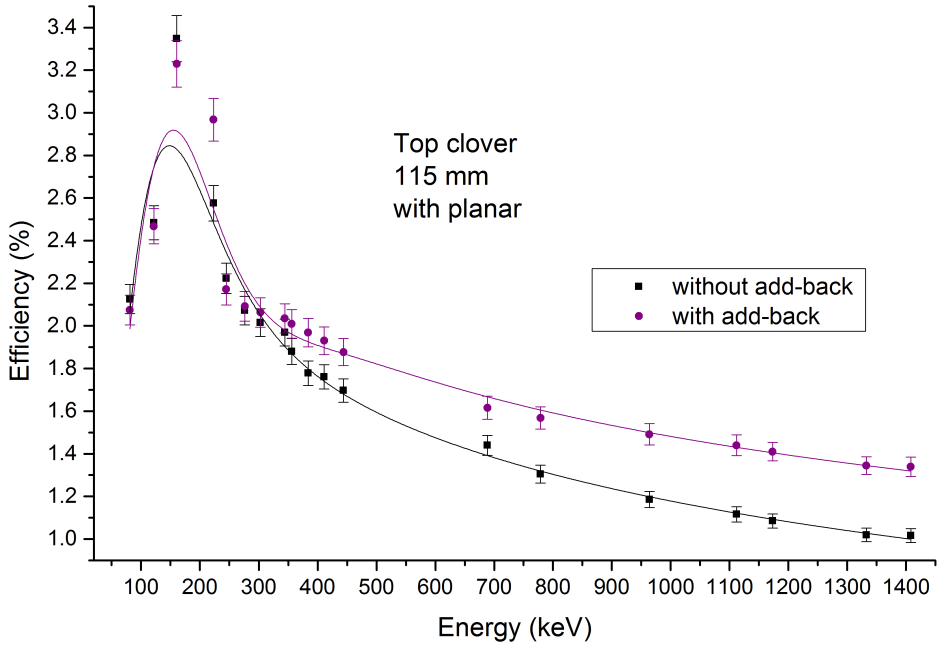

Figure 2.7: Absolute efficiency for the Top Clover detector. The relative position of the frame is 115 mm, the setup is equipped with planar detector.

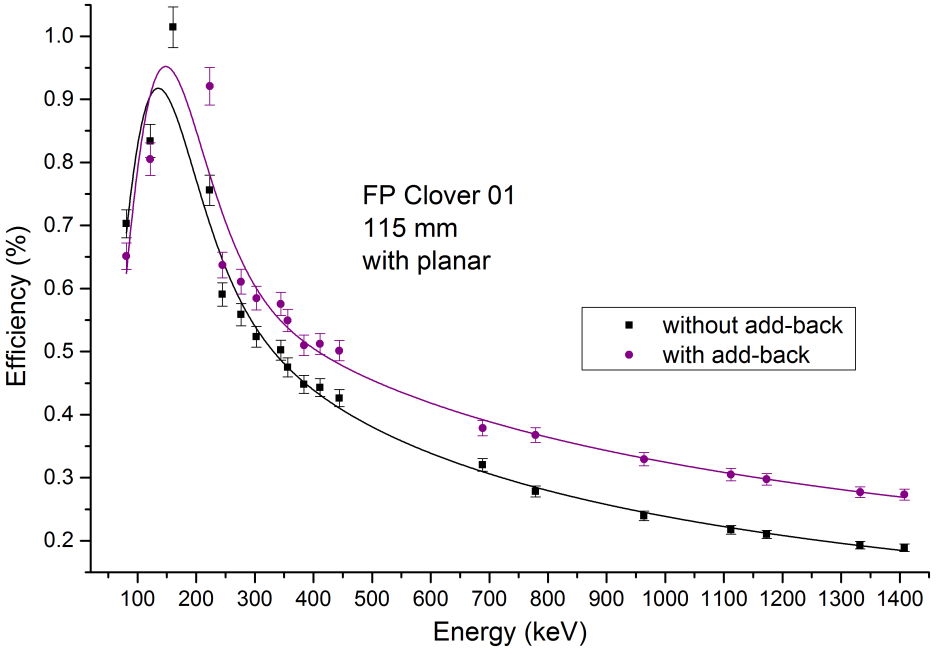

Figure 2.8: Absolute efficiency for the FPClover 01 detector. The relative position of the frame is 115 mm, the setup is equipped with planar detector.

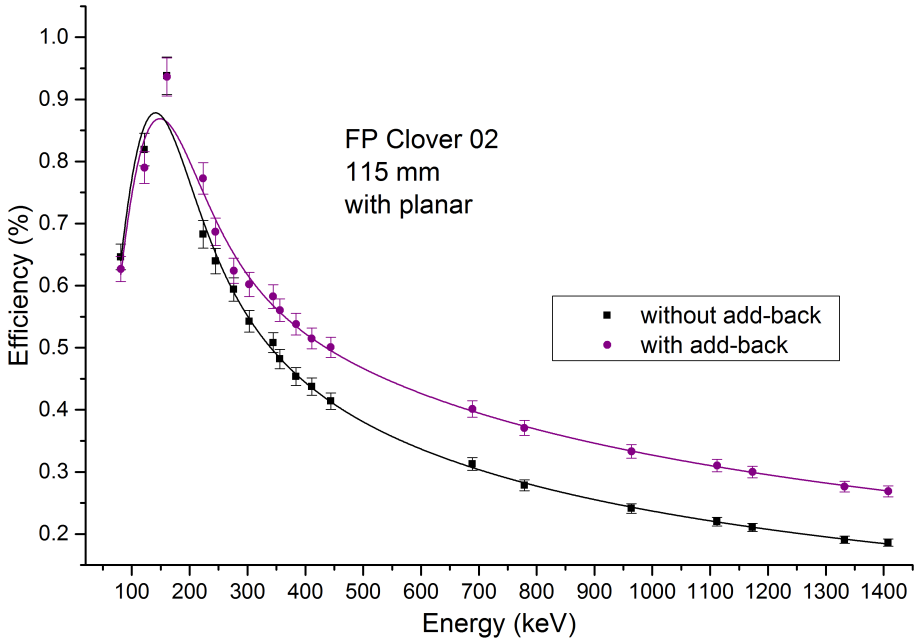

Figure 2.9: Absolute efficiency for the FPClover 02 detector. The relative position of the frame is 115 mm, the setup is equipped with planar detector.

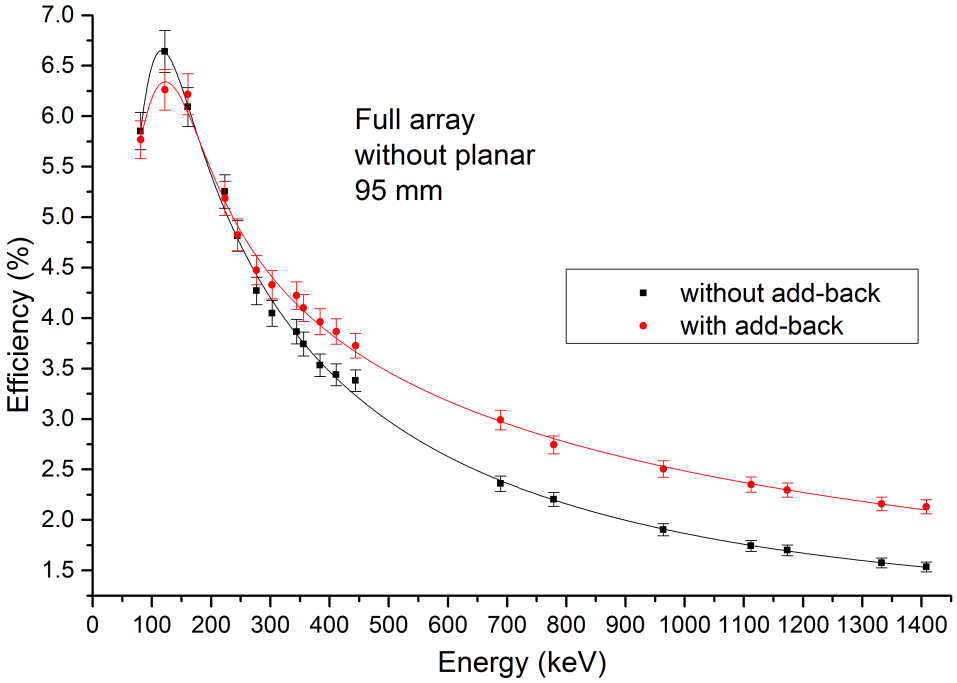

Figure 2.10: Absolute efficiency for the array of 3 clover detectors. The relative position of the frame is 95 mm, the setup is without planar detector.

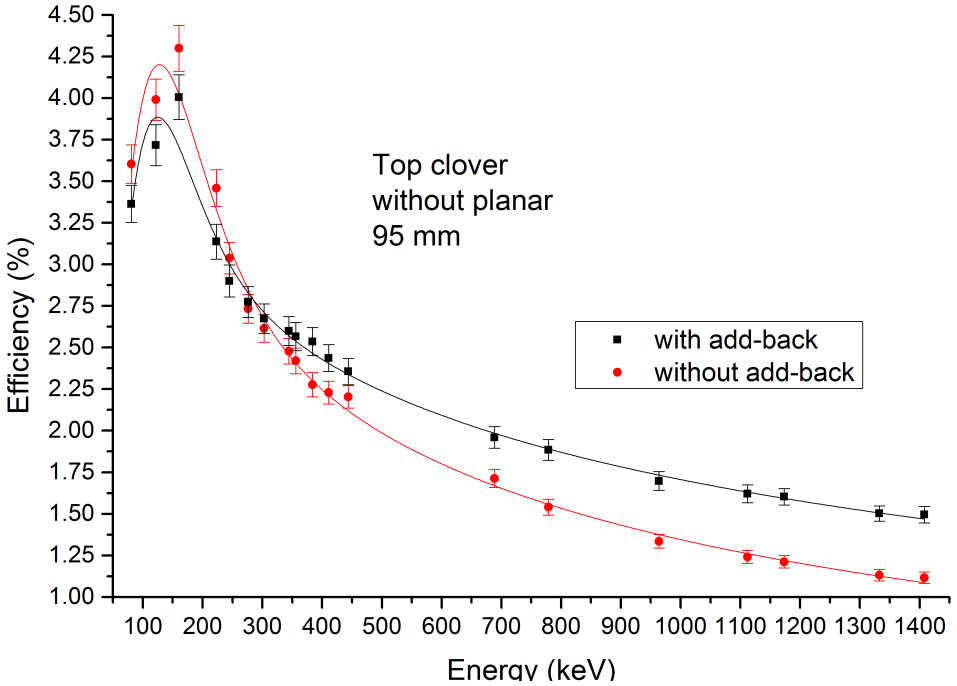

Figure 2.11: Absolute efficiency for the Top Clover detector. The relative position of the frame is 95 mm, the setup is without planar detector.

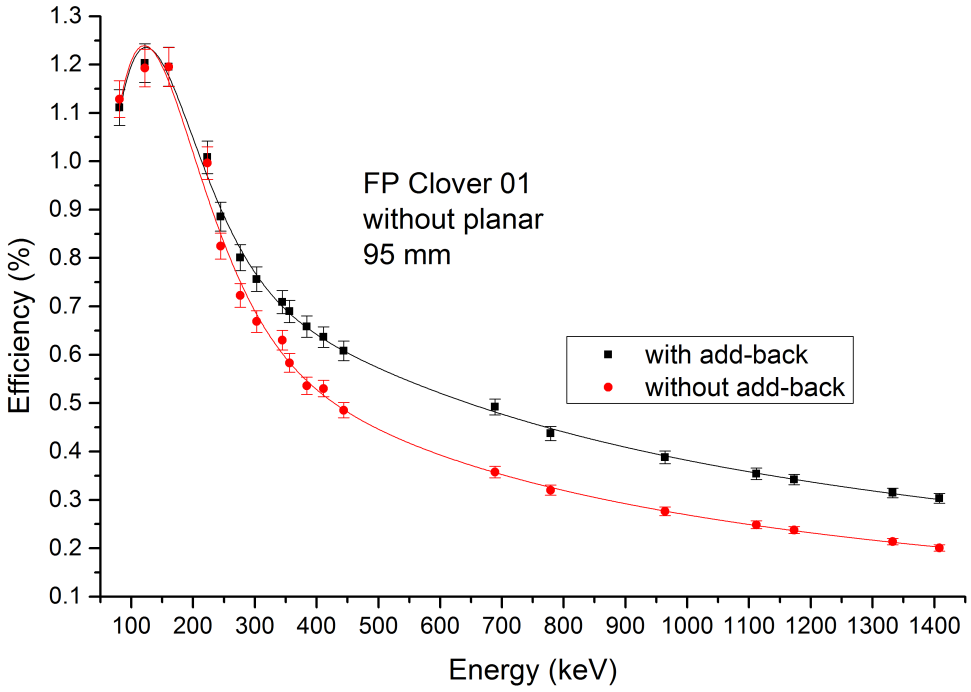

Figure 2.12: Absolute efficiency for the FPClover 01 detector. The relative position of the frame is 95 mm, the setup is without planar detector.

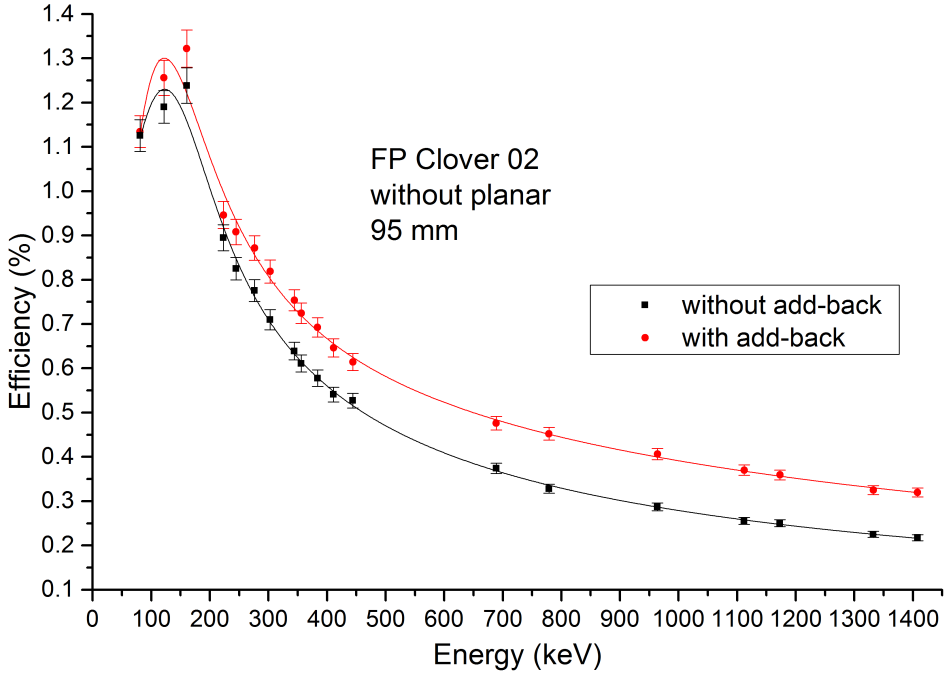

Figure 2.13: Absolute efficiency for the FPClover 02 detector. The relative position of the frame is 95 mm, the setup is without planar detector.

	Array		**Top Clover**	
	with AB	w/o AB	with AB	w/o AB
A	10.440	36.749	8.013	9.218
B	0.003	0.009	4.095	0.011
C	1.322	1.148	1.985	1.035
D	0.302	0.875	0.439	0.433
E	0.240	0.182	0.194	0.225
F	$-7.5 \cdot 10^{-}6$	$-1.5 \cdot 10^{-}6$	$-1.7 \cdot 10^{-}4$	$-3.9 \cdot 10^{-}5$
G	2.499	2.737	1.650	2.111
R^2	0.987	0.996	0.908	0.964

Table 2.1: Coefficients of the fitting equation for the array of detectors and for the Top Clover. The configuration is with the planar detector; the relative position of the frame is 115 mm.

	FPClover 01		**FPClover 02**	
	with AB	w/o AB	with AB	w/o AB
A	2.641	5.109	3.774	7.362
B	5.769	0.011	0.021	0.089
C	1.554	1.070	0.942	0.710
D	0.366	0.593	0.521	0.815
E	0.252	0.237	0.223	0.208
F	$-1.7 \cdot 10^{-}5$	$-8.4 \cdot 10^{-}6$	$-1.8 \cdot 10^{-}5$	$-9.2 \cdot 10^{-}6$
G	2.221	2.413	2.265	2.432
R^2	0.945	0.982	0.990	0.995

Table 2.2: Coefficients of the fitting equation for the side clovers. The configuration is with the planar detector; the relative position of the frame is 115 mm.

	Array		**Top Clover**	
	with AB	w/o AB	with AB	w/o AB
A	2987.064	64.305	11.563	19.973
B	1.220	0.657	0.008	0.019
C	0.383	0.250	1.126	0.971
D	4.406	16.872	0.417	0.577
E	0.068	-0.166	0.220	0.223
F	$-3.7 \cdot 10^{-}5$	$-9.7 \cdot 10^{-}5$	$-8.58 \cdot 10^{-}5$	$-6.39 \cdot 10^{-}5$
G	2.228	2.119	2.018	2.029
R^2	0.996	0.997	0.988	0.992

Table 2.3: Coefficients of the fitting equation for the array of detectors and for the Top Clover. The configuration is without the planar detector.

	FPClover 01		**FPClover 02**	
	with AB	w/o AB	with AB	w/o AB
A	3.592	5.472	4.992	$1.932 \cdot 10^{1}1$
B	$6.9 \cdot 10^{-}4$	0.002	0.086	16.655
C	1.487	1.283	0.670	0.097
D	0.290	0.488	0.546	22.648
E	0.295	0.263	0.222	0.026
F	$-1.16 \cdot 10^{3}$	$-6.2 \cdot 10^{-}4$	$-1.16 \cdot 10^{-}4$	$-1.02 \cdot 10^{-}5$
G	1.319	1.421	1.996	2.422
R^2	0.997	0.995	0.993	0.997

Table 2.4: Coefficients of the fitting equation for the sides detectors. The configuration is without the planar detector.

Chapter 3

Discussion

For most of the plots the fitting function does not match for a few experimental points at the highest region of the efficiency curve. This is because of the difficulties in determining the integration value of the peaks that correspond to these points. The reason for this circumstance is the low intensity of the transition that caused the γ-ray of this energy, in other words these peaks are very small compared with neighboring peaks. Another observation is that in some figures the add-back efficiency curves are lower than curves obtained without application of the add-back in the region of the low-energy γ-rays. This happens because the add-back algorithm falsely identifies the low energy peaks and adds them back, hence lowering the efficiency.

Monte-Carlo simulations have been performed by another M.Sc. student (Tuomas Taimi, University of Jyväskylä) utilizing GEANT4 (GEometry ANd Tracking), which is a toolkit for the simulation of the passage of particles through matter developed by CERN and written in C++. The simulation was done for the current configuration of the GREAT spectrometer and all distances and dimensions of the detectors at the GREAT spectrometer have been taken into account. Both cases of the assembly (with planar detector and without planar detector) were simulated, but the position of the moveable frame was constant: 109 mm, which places the DSSD at the center point of all the Clover detectors. The data obtained by the aid of simulation developed by T.Taimi have been analyzed without the application of an add-back algorithm, whereas the experimental data have been analyzed both with and without an add-back algorithm.

Efficiency curves obtained with the aid of the GEANT4 simulation are placed in the plots in the current chapter with experimental curves obtained without the add-back algorithm (Fig. 3.1- 3.8). The experimental results are in good agreement for the side detectors, but not for the Top Clover detector and therefore for the array of the detectors, since the Top Clover contributes

more than both side detectors together. For the Top Clover the simulation curve is higher than experimental one in the region of low energies (from 30 keV to 600-800 keV) and lower in the region of high energies (from 600-800 keV to 1400 keV).

Considering the experimental efficiency curves (Fig. 3.9 - 3.12) that were obtained two years before with analog electronics by summer student Matti Johannes Väisänen (University of Jyväskylä, [13]), one can see that the present investigation has been made with higher accuracy. In addition, digital electronics were used, resulting in an increase in efficiency by a factor of about 1.5. This result was expected, since for the present investigation data were collected for a longer time and the fitting was performed with specialized software. In addition, the utilization of digital electronics improves the low energy threshold, which increases the measurement efficiency for low energy γ-rays < 150 keV. The previous investigation [13] was made only with the planar detector installed and the conclusion about the optimal position were made in favor of 105 mm, that was taken as a compromise between two values of movable frame position, namely 100 mm and 110 mm and correspondingly two methods of determination of efficiency. However, the present research shows that the highest efficiency can be reached at the position 115 mm rather than at the position 105 mm, when the planar detector is installed. This could mean that in reality the optimal position of the movable frame is 110 mm, it should be underlined that there is a very strong reason for this assumption: when the center of any of clover detectors is on the level of DSSD this position corresponds to the frames relative position being 109 mm.

Comparing the present results with the simulation result obtained by A. Andreyev et al. (University of Liverpool, [24]) for the GREAT spectrometer, the following observation can be made: the experimental efficiency curves for the side clovers are in a good agreement with the simulated curves (Fig. 3.13), but the simulated efficiency curve for the Top Clover detector is higher than the experimental curve. This simulation has been performed taking into account different configuration of the experimental setup: there was another (fourth) clover detector behind the planar detector, also the position of the clover detectors relative to the DSSSD detector is not mentioned in the publication, most likely it was as in the recent simulation: 109 mm. Another distinction between the present result and result of the reference [24] is that in their simulation all three Ge-detectors were the same type as the Top Clover detector.

The absolute efficiency as function of γ-ray energy must fit to the exponential function Eq. 2.1 as is typical for HPGe-detectors [22]. The shape of the curve is determined not only by the detector characteristics, but also by

geometry of the set up and absorption effects and the associated electronics used to read out the signals. The differences between the Top Clover detector and one of the side detectors are in their location and also in their sizes, since the Top Clover detector crystals are about 2 times larger than the side detectors. The indicated difference is reflected in the shape of the efficiency curve (Fig. 3.14): this is a difference between the efficiency in the low-energy range and high-energy range.

The difference between the efficiency curves obtained by applying an add-back algorithm and without its application for the Top Clover detector is less than for the side detectors: for example, it is 1.32 times for the Top detector (Fig. 2.7 and 2.11) and in 1.43 times for the FPClover 01 (Fig. 2.8, 2.9 and 2.12, 2.13) for the particular case when the planar detector was removed and the position of the detector array was 95 mm. This effect is observed, because the larger size of the Top detector allows one to have more full energy absorption of γ-rays without the Compton scattering from one crystal to another, than in smaller side detectors, for which add-back algorithm gives a greater improvement for the efficiency.

Concluding this chapter, the present results do not contradict the previous researches and were made precisely enough (the correlation coefficients for all the fitted curves were close to 1). The results do not match completely to the results from other papers, because it was done with different equipment. Both simulation sets do not investigate what would be the optimal position for the movable frame with Ge-detectors, and another experimental research which investigated the optimal position was not made with the data acquisition system, which is in use. For the experimental setup equipped with the planar detector the assumption can be made, if the present results and previous results [13] are compared: the optimal position is 109-110 mm, which corresponds to the position of the center of any of the clover detectors on the level of the DSSSD implantation detector.

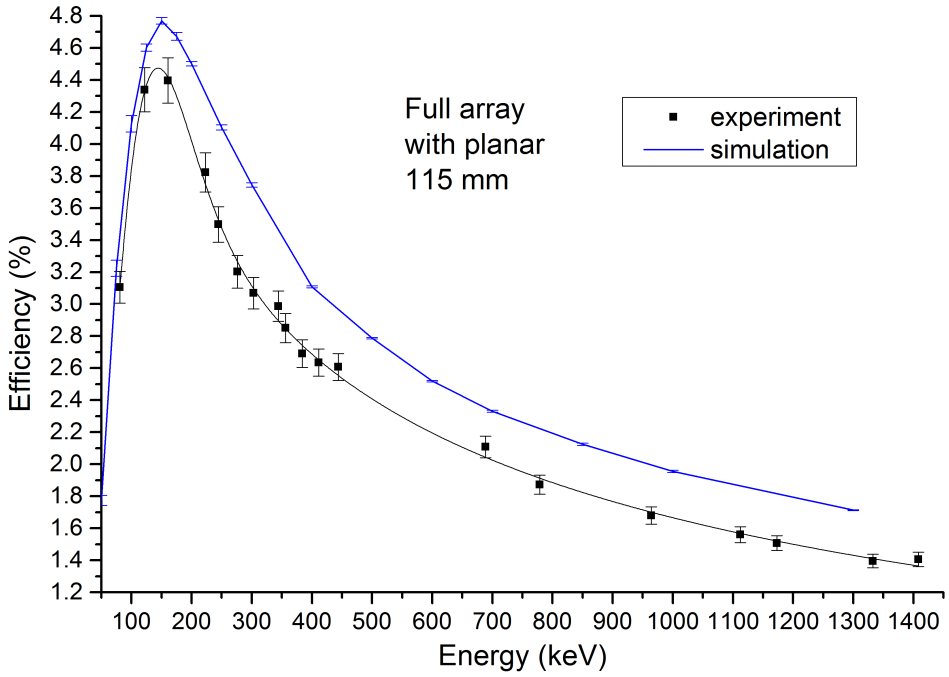

Figure 3.1: Absolute efficiency for the array of 3 clover detectors comparing with simulated data. The relative position of the frame is 115 mm, the setup is equipped with planar detector.

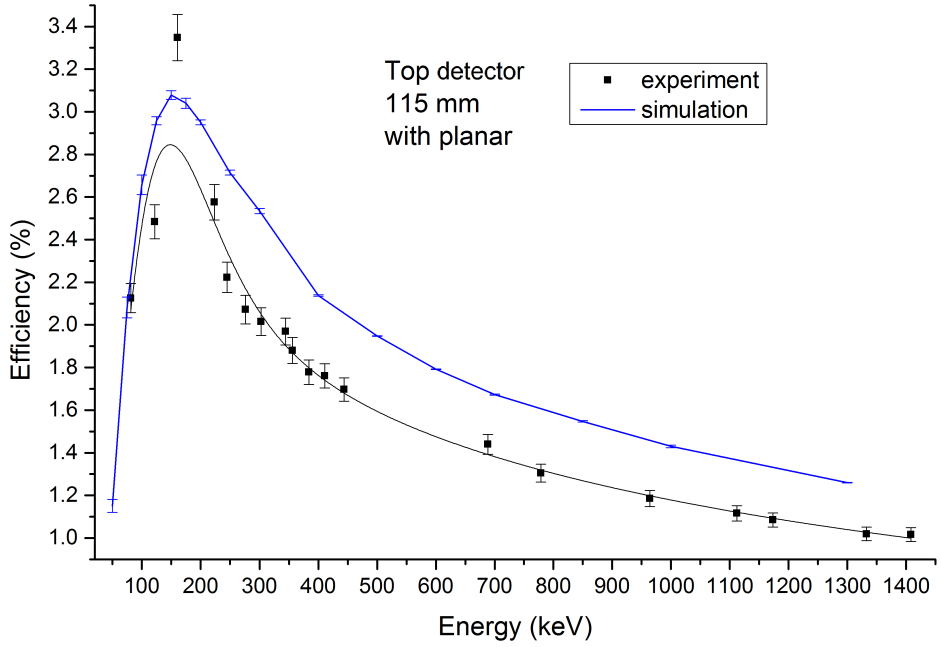

Figure 3.2: Absolute efficiency for the Top Clover detector comparing with simulated data. The relative position of the frame is 115 mm, the setup is equipped with planar detector.

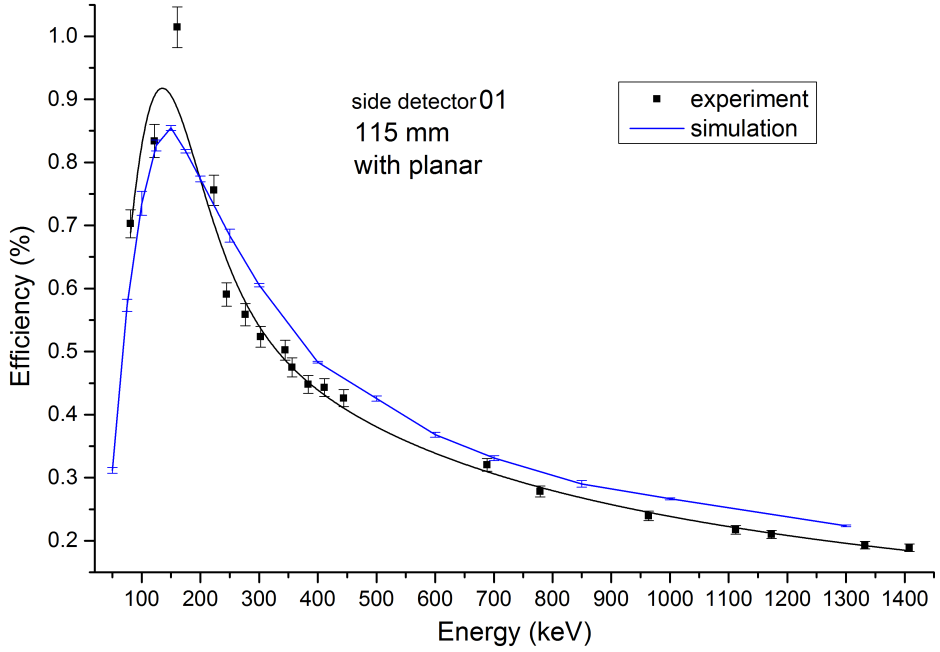

Figure 3.3: Absolute efficiency for the FPClover 01 detector comparing with simulated data. The relative position of the frame is 115 mm, the setup is equipped with planar detector.

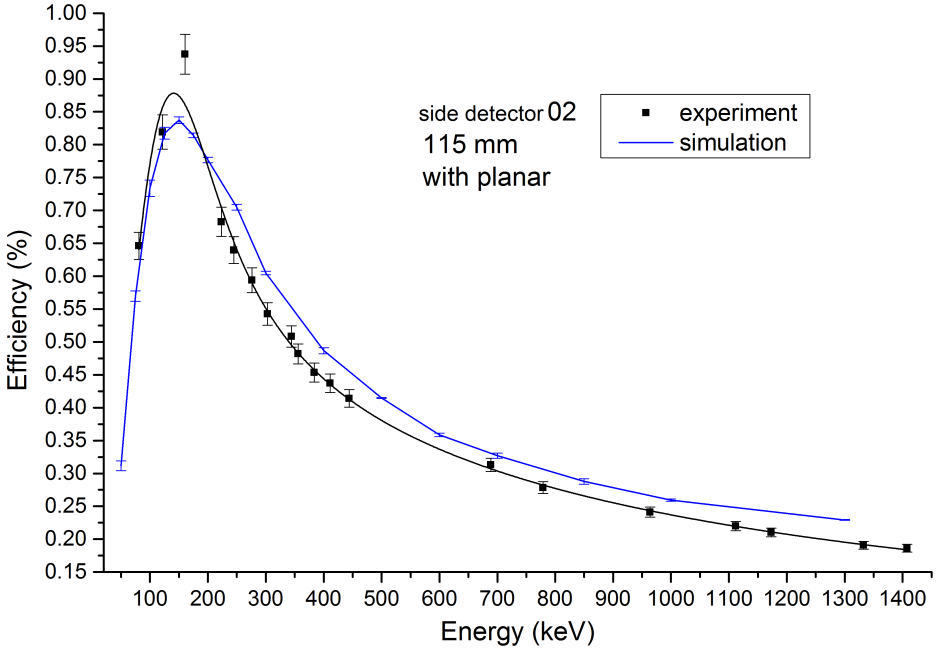

Figure 3.4: Absolute efficiency for the FPClover 02 detector comparing with simulated data. The relative position of the frame is 115 mm, the setup is equipped with planar detector.

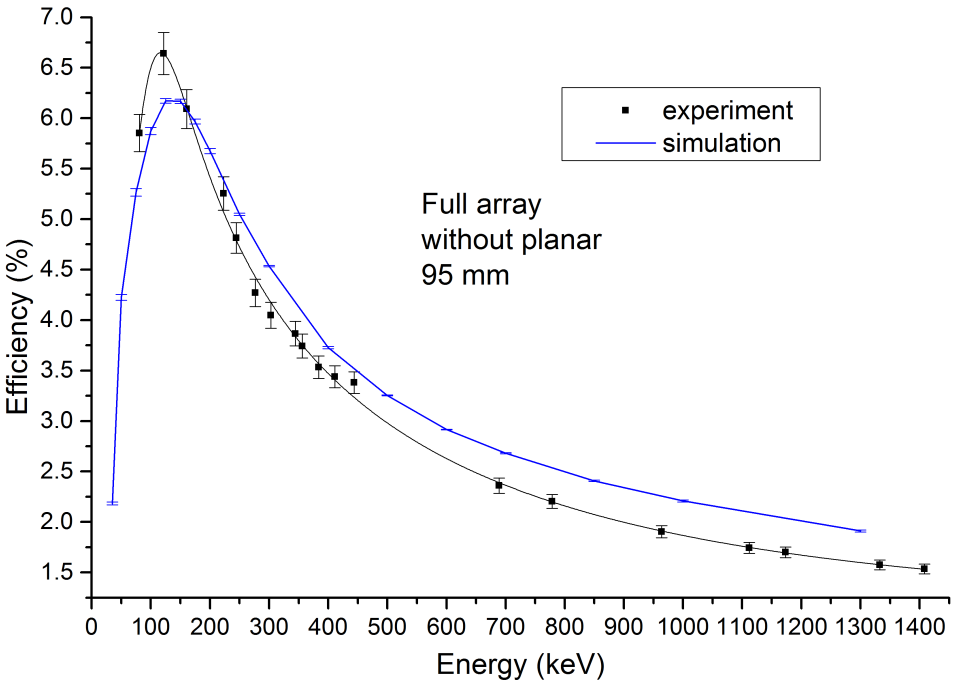

Figure 3.5: Absolute efficiency for the array of 3 clover detectors comparing with simulated data. The relative position of the frame is 95 mm, the setup is without planar detector.

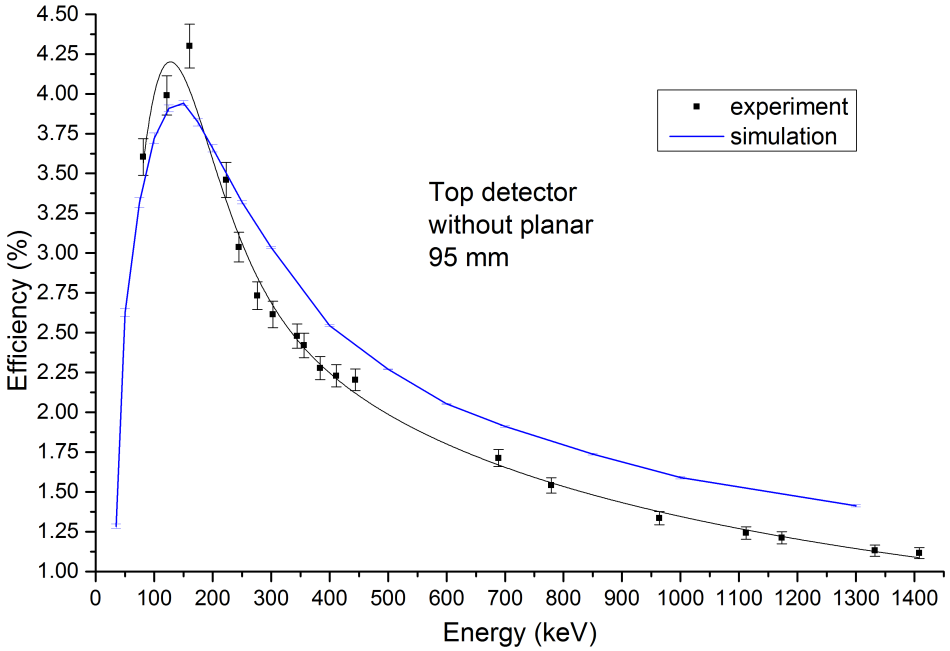

Figure 3.6: Absolute efficiency for the Top Clover detector comparing with simulated data. The relative position of the frame is 95 mm, the setup is without planar detector.

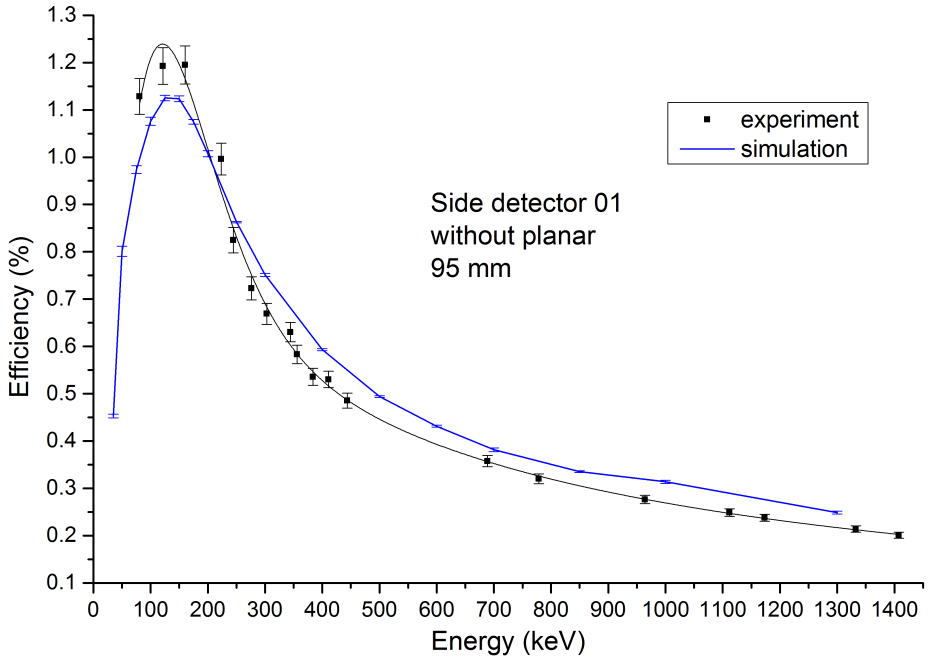

Figure 3.7: Absolute efficiency for the FPClover 01 detector comparing with simulated data. The relative position of the frame is 95 mm, the setup is without planar detector.

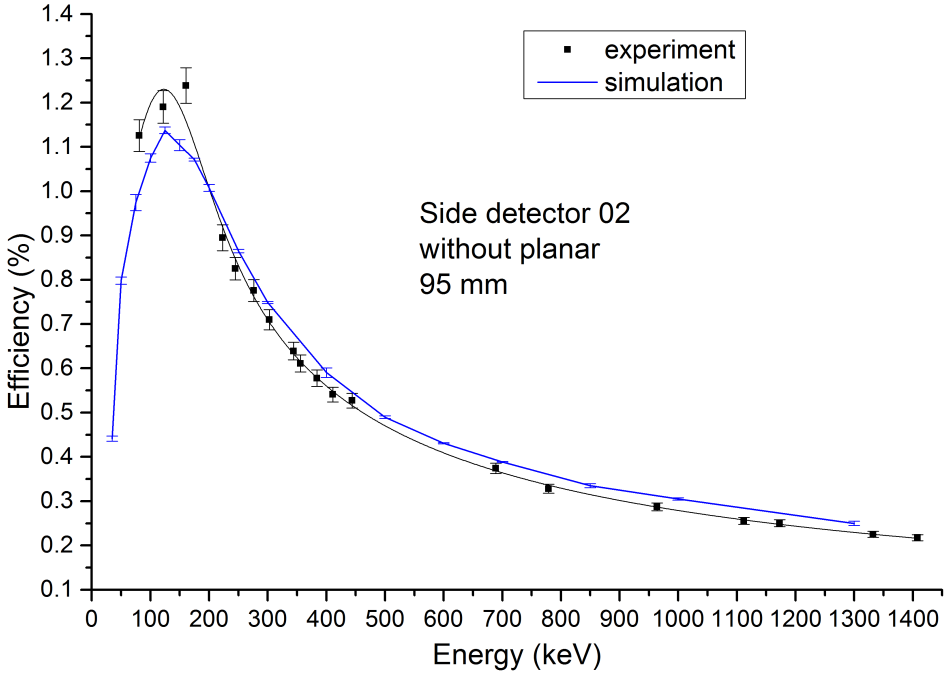

Figure 3.8: Absolute efficiency for the FPClover 02 detector comparing with simulated data. The relative position of the frame is 95 mm, the setup is without planar detector.

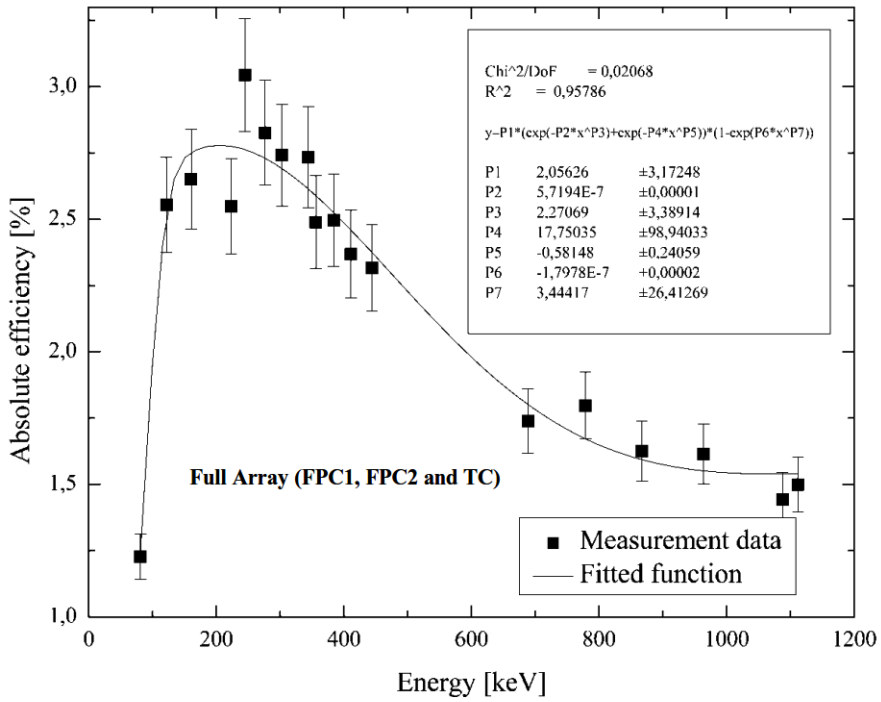

Figure 3.9: The efficiency curve obtained for the array of germanium detectors utilizing analog electronics [13].

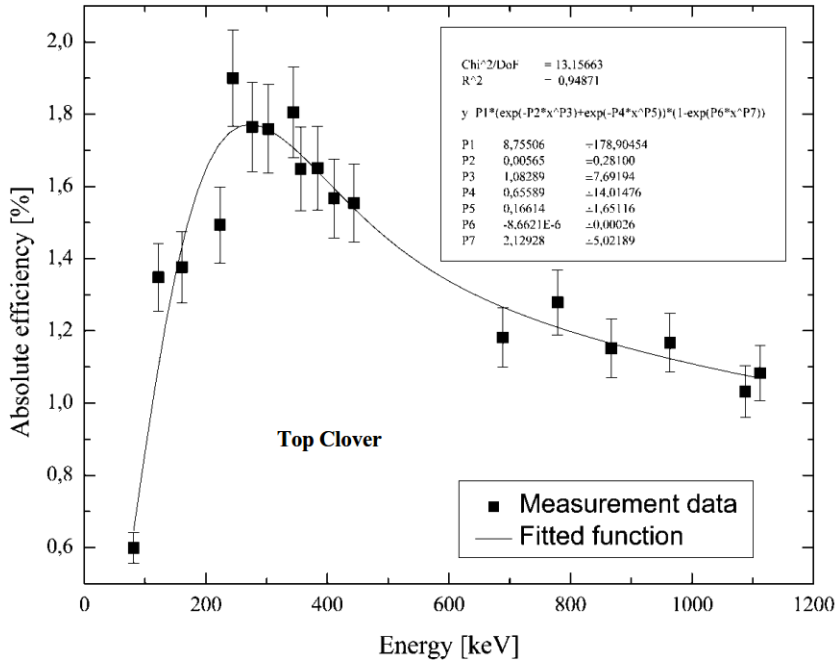

Figure 3.10: The efficiency curve obtained for the Top Clover detector utilizing analog electronics [13].

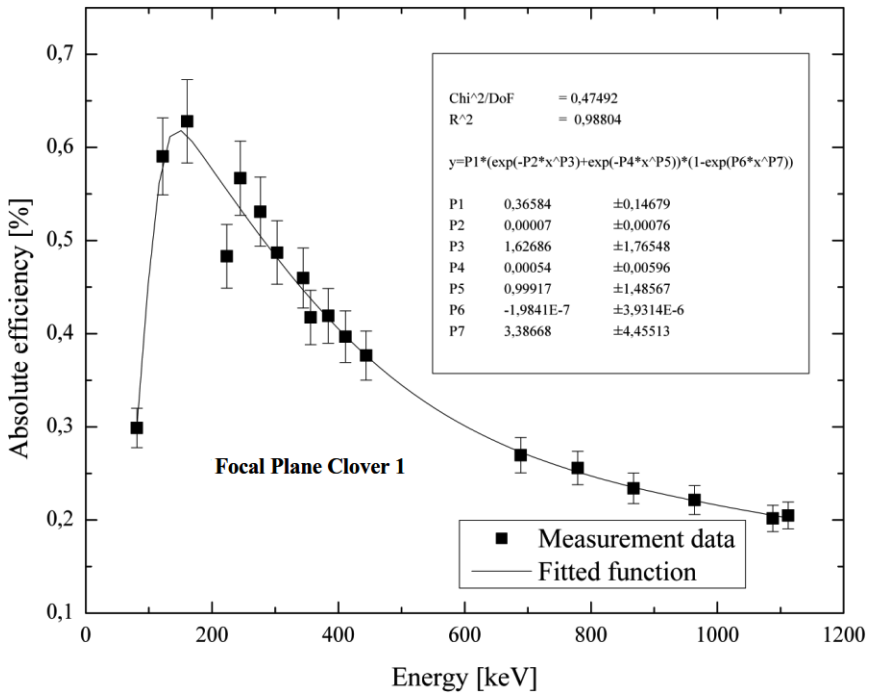

Figure 3.11: The efficiency curve obtained for the FPClover 01 detector utilizing analog electronics [13].

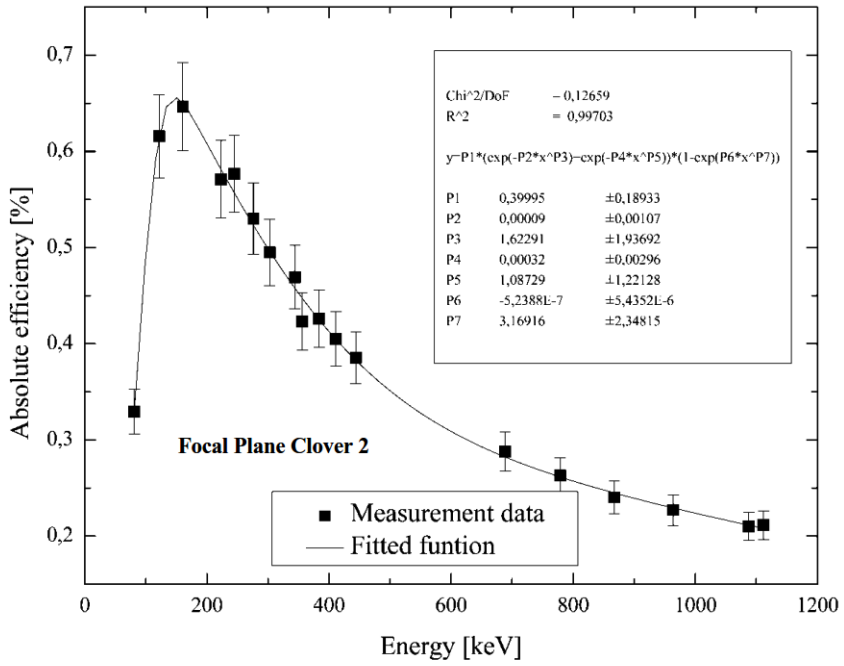

Figure 3.12: The efficiency curve obtained for the FPClover 02 detector utilizing analog electronics [13].

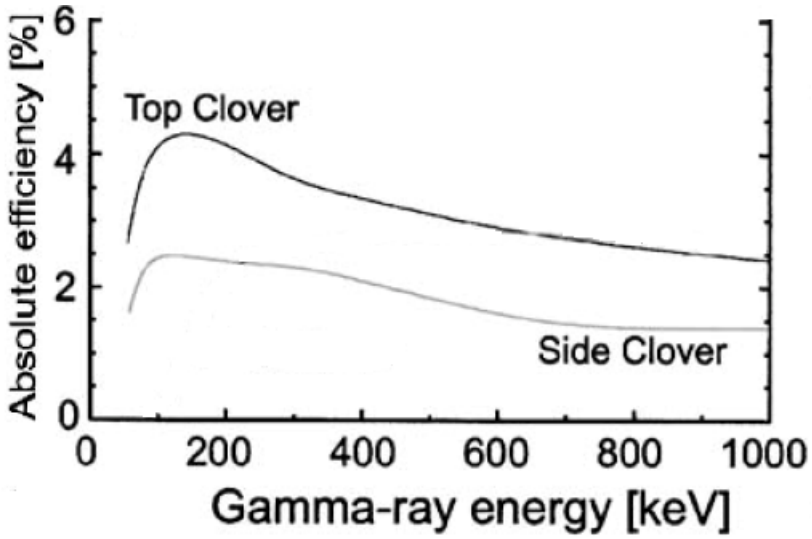

Figure 3.13: The simulation results obtained by Andreyev and others [24] for the configuration with planar detector, applying add-back method and with clover detector behind planar detector.

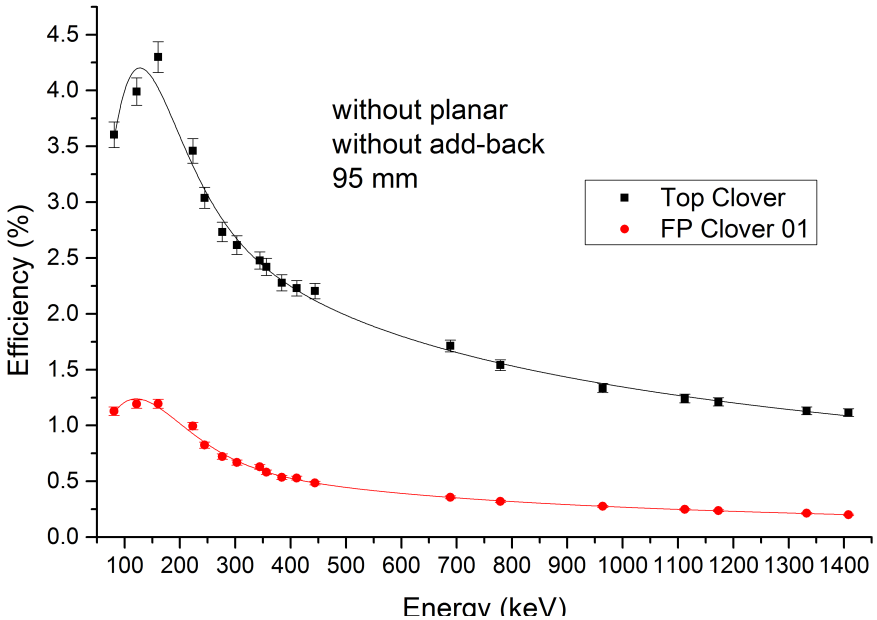

Figure 3.14: The efficiency curves for the top and side detectors for the case, when the planar detector was removed and position of the detectors array was 95 mm.

Conclusion

The efficiency curves for each detector independently and as an array were obtained as a result of this diploma work. The data have been analyzed both with and without application of an add-back algorithm. Experiments have been carried for two configurations of the GREAT spectrometer, namely with planar detector and without it. The application of the add-back algorithm provides a higher value of efficiency at higher energies. The experimental data were obtained with a precision of 3%. The efficiency curves were fitted with a good conformity with the data, judging by the correlation coefficients. The curves for the side clover detectors are in a good agreement with both simulations, whereas for the Top Clover detector the experimental data showed a lower efficiency, than was simulated.

The optimal relative position of the movable frame with clover Ge-detectors for both cases has been determined with accuracy 5 mm. An optimal position value of 95 mm was obtained for the present research, when the GREAT spectrometer is not equipped with planar detector, and 115 mm, when it is equipped with this detector. In prospect the comparison of efficiency curves for 105 mm, 110 mm and 115 mm need to be done by the aid of the simulation for the setup configuration with planar detector. It is found that the planar detector can be removed from the GREAT spectrometer for those experiments, when there is no need to detect x-rays and low energy γ-rays, since the efficiency of all three clover Ge-detectors is higher in such a configuration.

The obtained efficiency curves will be used to improve the simulation code for the GREAT spectrometer, especially for the Top Clover detector, then it can be very useful for testing the different configuration of the spectrometer without occupying the laboratory equipment and space for it. The obtained efficiency will be useful for future experiments to estimate the γ-ray transition intensity and consequently a spin-parity of the state and the type of the transition, which is important for the nuclear structure studies.

Bibliography

[1] K. Szymańska, P. Achenbach, M,. Agnello et al. *Resolution, efficiency and stability of HPGe detector operating in a magnetic field at various gamma-ray-energies* Nuclear Instruments and Methods in Physics Research A 592 (2008) 486-492

[2] J. Simpson *The Euroball spectrometer* Zeitschrift für Physik A Atomic Nuclei 01/1997

[3] G.de Angelis, A. Bracco, D. Curien *The EUROBALL gamma ray detector array* Europhysics News 34 (2003) 181-185

[4] M.A. Deleplanque, R.M. Diamonds *Gammasphere Proposal* Lawrence Berkeley Laboratory, Report 5202, 1988

[5] J. Simpson *The AGATA spectrometer* Acta Physica Polonica B 36 (2005) 1383-1393

[6] M. Leino, J. Äystö, T. Enqvist, P. Heikkinen, A. Jokinen, M. Nurmia, A. Ostrowski, W.H. Trzaska, J. Uusitalo, K. Eskola, P. Armbruster, V. Ninov *Gas-filled recoil separator for studies of heavy elements* Nuclear Instruments and Methods in Physics Research B 99 (1995) 653-656

[7] M. Leino *In-flight separation with gas-filled systems*, Nuclear instruments and methods in physics research, Section B: Beam interactions with material and atoms, 126(1-4):320-328 (1997) `http://www.sciencedirect.com/science/article/pii/S0168583X96010014`

[8] *GREAT: Studies of Nuclei far from Stability by Tagging Techniques* `http://npg.dl.ac.uk/GREAT/`, 2004

[9] C. Scholey *The GREAT spectrometer* `https://www.jyu.fi/fysiikka/en/research/accelerator/nucspec/GREAT/`, 2006

[10] P. Peura *Spectroscopic studies of ^{173}Pt and ^{175}Pt*, Department of Physics, University of Jyväskylä, Finland, research report No. 13/2014

[11] Andrei Andreyev *GEANT-calculations for the GREAT set-up* `http://npg.dl.ac.uk/GREAT/geant_gr.htm`, 2004

[12] *The technical description of GREAT* `http://npg.dl.ac.uk/GREAT/Technical_Description.pdf`, 2004

[13] Matti Väisänen *Optimization of RITU focal plane clover detector system*, JYFL, 2012

[14] J. Llacer *Planar and coaxial high purity germanium radiation detectors* Nuclear Instruments and Methods 98, 259 (1972)

[15] I.H. Lazarus et al. *The GREAT triggerless Total Data Readout method* IEEE Transactions on nuclear science, vol. 48, No.3, June 2001

[16] V. Pucknell, S.Letts *Data acquisition software MIDAS* `http://npg.dl.ac.uk/MIDAS/`, Daresbury, UK

[17] P. Rahkila *Grain - a Java data analysis system for Total Data readout* Nuclear Instruments and Methods in Physics Research A 595 (2008) 637

[18] Glenn F. Knoll *Radiation detection and measurement* 4th edition, Wiley, USA, 2010

[19] W.H. Trzaska *Recommended data on selected gamma-ray and conversion-electron calibration sources* Nuclear Instruments and Methods in Physics Research A 297 (1990) 223-229

[20] Schötzig U. and Schrader H. *Halbwertszeiten und Photonen-Emissionwahrscheinlichkeiten von häufig verwendeten Radionukliden*, PTB-Bericht, PTB-Ra-16/5, Braunschweig, September 1998

[21] D.C. Radford *Notes on the useof the program gf3*, Oak RidgeNational Laboratory, May 2000

[22] S. Hurtado, M. Garcia-Leon, R. Garcia-Tenorio *A fitting algorithm based on simulated annealing techniques for efficiency calibration of HPGe detectors using different mathematical functions* Nuclear Instruments and Methods in Physics Research A 594 (2008) 362-367

[23] Origin web-page `http://www.originlab.com/`

[24] A.N. Andreyev, P.A. Butler, R.D. Page, D.E. Appelbe, G.d. Jones, D.T. Joss, R.-D Herzberg, P.H. Regan, J. Simpson, R. Wadsworth *GEANT Monte Carlo simulations for the GREAT spectrometer* Nuclear Instruments and Methods in Physics Research A 533 (2004) 422-434

Appendices

Appendix A

The sorting code

```
import fi.jyu.phys.grain.sort.*;
import fi.jyu.phys.grain.sort.detector.*;
import fi.jyu.phys.grain.sort.gates.*;
import fi.jyu.phys.grain.resources.GrainConstants;
import hep.aida.*;
import java.util.*;
import java.text.NumberFormat;

public class eff_test_clo2 extends GrainGreatSorter {


    /*-----------------------------------------------
     * Name gates
     *-----------------------------------------------*/

    GrainGate1D tgate2;

    /*-----------------------------------------------
     * Placeholders for stuff...
     *-----------------------------------------------*/

    NumberFormat nf2;
    GrainDetectorGermaniumArray focalplanearray;

    /*-----------------------------------------------
     * Initialise the sort
     *-----------------------------------------------*/
    public void initialise() {
```

```
        nf2 = NumberFormat.getInstance();
        nf2.setMaximumIntegerDigits(2);
        nf2.setMinimumIntegerDigits(2);
        nf2.setGroupingUsed(false);

/*-----------------------------------------------
* Define spectrum names and binning
*-----------------------------------------------*/
create_planar();
create_cloverG();
create_clover();

/*-----------------------------------------------
 * Set Gate Limits
 *-----------------------------------------------*/
tgate2 = new GrainGate1D(-20000,20000); //Add-back for FParray


    }

    /*-----------------------------------------------
     * Event Handler
     *-----------------------------------------------*/
    public void process() {

do_planar();
do_cloverG();
do_clover();

focalplanearray = construct_fparray(tgate2, true, false);
event.store.put("FParray", focalplanearray);
    }



    /*-----------------------------------------------
     * Planar GE spectra
     *-----------------------------------------------*/
    IHistogram1D planary,planarx;
    IHistogram1D planarsx, planarsy;
```

```
    IHistogram1D px[];
    IHistogram1D py[];
    private void create_planar(){
tree.mkdir("Planar calibrated");
tree.cd("Planar calibrated");
planarsx = hfactory.createHistogram1D("Planar X Energy,
1keV bin",1000,0,1000);
planarsy = hfactory.createHistogram1D("Planar Y Energy,
1keV bin",1000,0,1000);
tree.mkdir("Strips");
tree.cd("Strips");
px = new IHistogram1D[24];
for(int i=0;i<px.length;i++){
px[i] = hfactory.createHistogram1D("Planar X Energy "
+nf2.format(i+1)+", 1keV bin",4096,0,4096);
}
py = new IHistogram1D[12];
for(int i=0;i<py.length;i++){
py[i] = hfactory.createHistogram1D("Planar Y Energy "
+nf2.format(i+1)+", 1keV bin",4096,0,4096);
}
tree.cd("..");
tree.cd("..");
    }

    private void do_planar(){
for( GrainDetectorStrip s : event.planar.xstrips){
planarsx.fill(s.value);
px[s.coord].fill(s.value);
}

for( GrainDetectorStrip s : event.planar.ystrips ) {
planarsy.fill(s.value);
py[s.coord].fill(s.value);
}
    }

    /*-----------------------------------------------
     * Great Clover spectra
     *-----------------------------------------------*/
    IHistogram1D cloverGtot;
```

```
    IHistogram1D ccG[];
    IHistogram2D cloverGmap;
    private void create_cloverG(){
tree.mkdir("Great Clover calibrated");
tree.cd("Great Clover calibrated");
cloverGtot = hfactory.createHistogram1D("Great Clover Total,
1keV bin",2000,0,2000);
tree.mkdir("CrystalsG");
tree.cd("CrystalsG");
ccG = new IHistogram1D[4];
for(int i=0;i<ccG.length;i++){
ccG[i] = hfactory.createHistogram1D("Great Clover Crystal Energy "
+(i+1)+", 1keV bin",2000,0,2000);
}
tree.cd("..");
tree.cd("..");
    }

    private void do_cloverG(){
for( GrainDetectorCloverCrystal c : event.clover.crystals){
cloverGtot.fill(c.e);
ccG[c.number].fill(c.e);
}
    }

    /*-----------------------------------------------
     * FPClover spectra
     *-----------------------------------------------*/
    IHistogram1D clovertot, fp01clo, fp02clo, top_clo;
    IHistogram1D cc[];
    IHistogram2D clovermap;
IHistogram1D fparray_wab, topClo_wab, fp01clo_wab, fp02clo_wab;
    private void create_clover(){
tree.mkdir("FParray calibrated");
tree.cd("FParray calibrated");
clovertot = hfactory.createHistogram1D("FParray Total,
1keV bin",2000,0,2000);
fp01clo = hfactory.createHistogram1D("FP Clover 01,
1keV bin",2000,0,2000);
fp02clo = hfactory.createHistogram1D("FP Clover 02,
1keV bin",2000,0,2000);
```

```
top_clo = hfactory.createHistogram1D("Top Clover,
1keV bin",2000,0,2000);

tree.mkdir("FParray with Addback");
tree.cd("FParray with Addback");
fparray_wab = hfactory.createHistogram1D("FP array Addback,
1 keV bin",3000,0,3000);
topClo_wab = hfactory.createHistogram1D("Top Clover Addback,
1 keV bin",3000,0,3000);
fp01clo_wab = hfactory.createHistogram1D("FP Clover 01 Addback,
1 keV bin",3000,0,3000);
fp02clo_wab = hfactory.createHistogram1D("FP clover 02 Addback,
1 keV bin",3000,0,3000);
tree.cd("..");

tree.mkdir("Crystals");
tree.cd("Crystals");
cc = new IHistogram1D[16];
for(int i=0;i<cc.length;i++){
cc[i] = hfactory.createHistogram1D("Clover Crystal Energy "+(i+1)+",
1keV bin",2000,0,2000);
}
tree.cd("..");
tree.cd("..");
    }

    private void do_clover(){
for( GrainDetectorGermanium c : event.fparray.ges){
clovertot.fill(c.e);
cc[c.number].fill(c.e);
if (c.number == 4 | c.number == 5 | c.number == 6 | c.number == 7){
fp01clo.fill(c.e);
}
if (c.number == 12 | c.number == 13 | c.number == 14 | c.number == 15){
fp02clo.fill(c.e);
}
if (c.number == 0 | c.number == 1 | c.number == 2 | c.number == 3){
top_clo.fill(c.e);
}
}
```

```
    }

    /*-----------------------------------------------
     * Finalise the sort
     *-----------------------------------------------*/
    public void finalise() {
    }

@SuppressWarnings({ "unchecked", "rawtypes" })
public GrainDetectorGermaniumArray construct_fparray(GrainGate1D
timegate, boolean diagonals, boolean allowbad) {

// Some variables
boolean valid,fail,pileup,veto;
double sum, max, theta, phi;
long t;

// The resulting Jurogam2 array
GrainDetectorGermaniumArray result2 =
new GrainDetectorGermaniumArray();

// Structure to fold out the clovers
ArrayList cclist[] = new ArrayList[24];
for(int i=0;i<cclist.length;i++){
cclist[i]= new ArrayList<GrainDetectorGermanium>(0);
}

// All the clover crystals to the correct location
//in the data structure
for( GrainDetectorGermanium ger: event.fparray.ges){
if(timegate.passes(ger.time-event.stamp)){
((ArrayList<GrainDetectorGermanium>)cclist[ger.number/4])
.add(ger);
}
}

// Loop over clover data
for(int i=0;i<cclist.length;i++){
// And process according to hit multiplicity
switch (cclist[i].size()){
case 1:
```

```
// Single hit case
// Pull out the hit
GrainDetectorGermanium ge =
((ArrayList<GrainDetectorGermanium>)cclist[i]).get(0);
// Create and store the new detector object
if((!ge.fail && !ge.piledup && !ge.vetoed) || allowbad)
result2.ges.add(new GrainDetectorGermanium(i+16,(i/12)+4,ge.theta,
ge.phi,ge.e,ge.time,1,ge.valid,ge.fail,ge.piledup,ge.vetoed));
break;
case 2:
// Double hit case
// Pull out the hits
GrainDetectorGermanium ge1 =
((ArrayList<GrainDetectorGermanium>)cclist[i]).get(0);
GrainDetectorGermanium ge2 =
((ArrayList<GrainDetectorGermanium>)cclist[i]).get(1);

// Non-diagonals and diagonals
int diff = Math.abs(ge1.number%4 - ge2.number%4);
if( !(diff == 2) ){
// Pick out the time from the higher energy
t = 0;
if(ge1.e > ge2.e) t = ge1.time;
else t=ge2.time;
// Calculate averages
theta = (ge1.theta+ge2.theta)/2.0;
phi = (ge1.phi+ge2.phi)/2.0;
// Create and store the new detector object
if((!ge1.fail && !ge1.piledup && !ge1.vetoed && !ge2.fail
&& !ge2.piledup && !ge2.vetoed) || allowbad)
result2.ges.add(new GrainDetectorGermanium(i+16,(i/12)+4,
theta,phi,ge1.e+ge2.e,t,2,ge1.valid&&ge2.valid,ge1.fail||ge2.fail,
ge1.piledup||ge2.piledup,ge1.vetoed||ge2.vetoed));
}
else if(diagonals){
// Diagonal hits
// Use as single hits at your own risk ...
if((!ge1.fail && !ge1.piledup && !ge1.vetoed) || allowbad)
result2.ges.add(new GrainDetectorGermanium(i+16,(i/12)+4,ge1.theta,
ge1.phi,ge1.e,ge1.time,1,ge1.valid,ge1.fail,ge1.piledup,ge1.vetoed));
if((!ge2.fail && !ge2.piledup && !ge2.vetoed) || allowbad)
```

```
result2.ges.add(new GrainDetectorGermanium(i+16,(i/12)+4,ge2.theta,
ge2.phi,ge2.e,ge2.time,1,ge2.valid,ge2.fail,ge2.piledup,ge2.vetoed));
}
break;
case 3:
// Triple hit case
// Accept everything
valid = true;
fail = pileup = veto = false;
sum = 0.0;
// Pick out the time from the highest energy
max = 0.0;
t = 0;
for(GrainDetectorGermanium geh:
((ArrayList<GrainDetectorGermanium>)cclist[i])){
sum += geh.e;
if(geh.e>max){
t=geh.time;
max=geh.e;
}
fail = fail || geh.fail;
pileup = pileup || geh.piledup;
veto = veto || geh.vetoed;
}
valid = (!fail && !pileup && !veto);
// Calculate angles
theta = 75.5+(double)(i/12)*29.0;
phi = (double)(i&12)*30.0+15.0;
// Create and store the new detector object
if(valid || allowbad)
result2.ges.add(new GrainDetectorGermanium(i+16,(i/12)+4,
theta,phi,sum,t,3,valid,fail,pileup,veto));
break;
case 4:
// Quad hit case
// Accept everything
valid = true;
fail = pileup = veto = false;
sum = 0.0;
// Pick out the time from the highest energy
max = 0.0;
```

```
t = 0;
for(GrainDetectorGermanium geh:
((ArrayList<GrainDetectorGermanium>)cclist[i])){
sum += geh.e;
if(geh.e>max){
t=geh.time;
max=geh.e;
}
fail = fail || geh.fail;
pileup = pileup || geh.piledup;
veto = veto || geh.vetoed;
}
valid = (!fail && !pileup && !veto);
// Calculate angles
theta = 75.5+(double)(i/12)*29.0;
phi = (double)(i&12)*30.0+15.0;
// Create and store the new detector object
if(valid || allowbad)
result2.ges.add(new GrainDetectorGermanium(i+16,(i/12)+4,
theta,phi,sum,t,4,valid,fail,pileup,veto));
break;
default:
break;
}
}

return result2;
}

}
```

Appendix B

Plots for measurements with planar detector

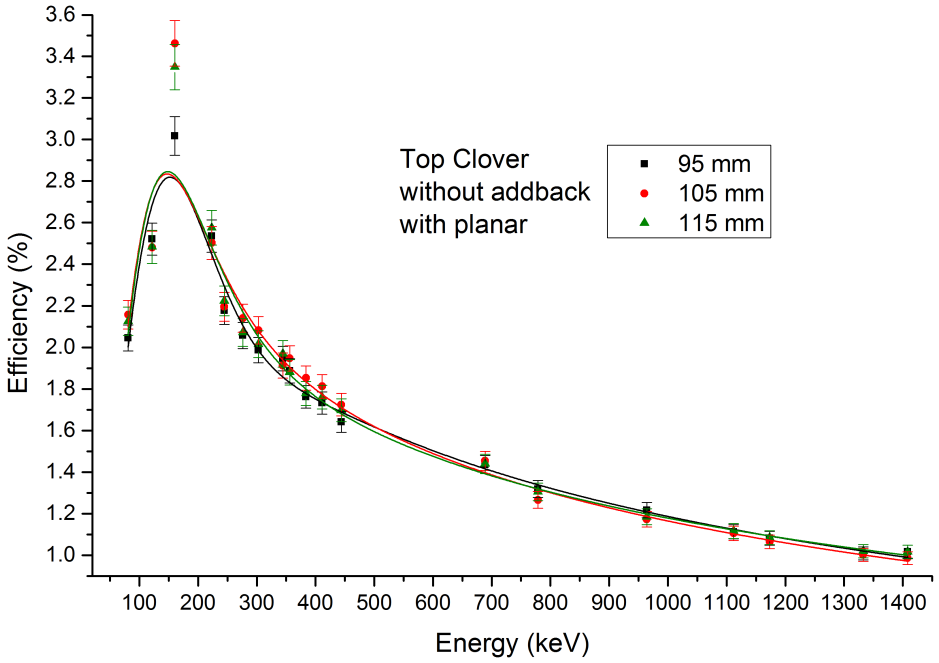

Figure B.1: Efficiency curves for Top Clover detector, without application add-back code.

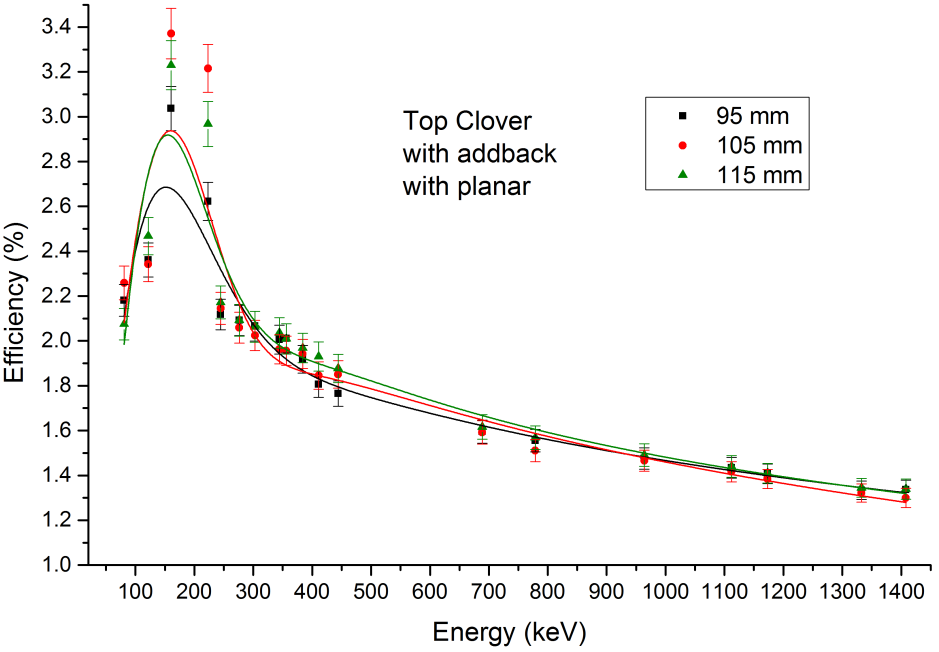

Figure B.2: Efficiency curves for Top Clover detector, applying add-back code.

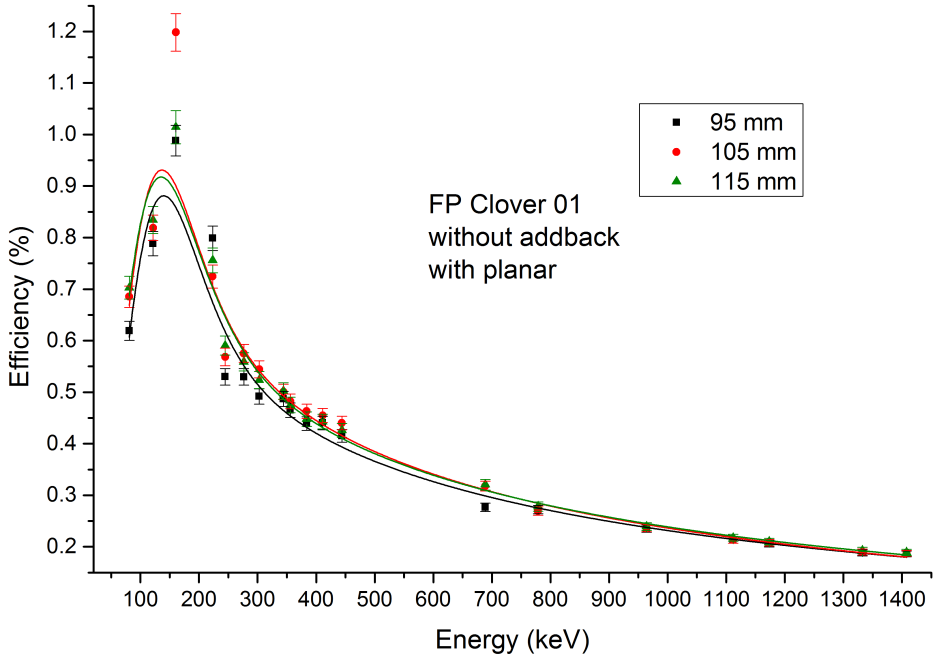

Figure B.3: Efficiency curves for FPClover01 detector, without application add-back code.

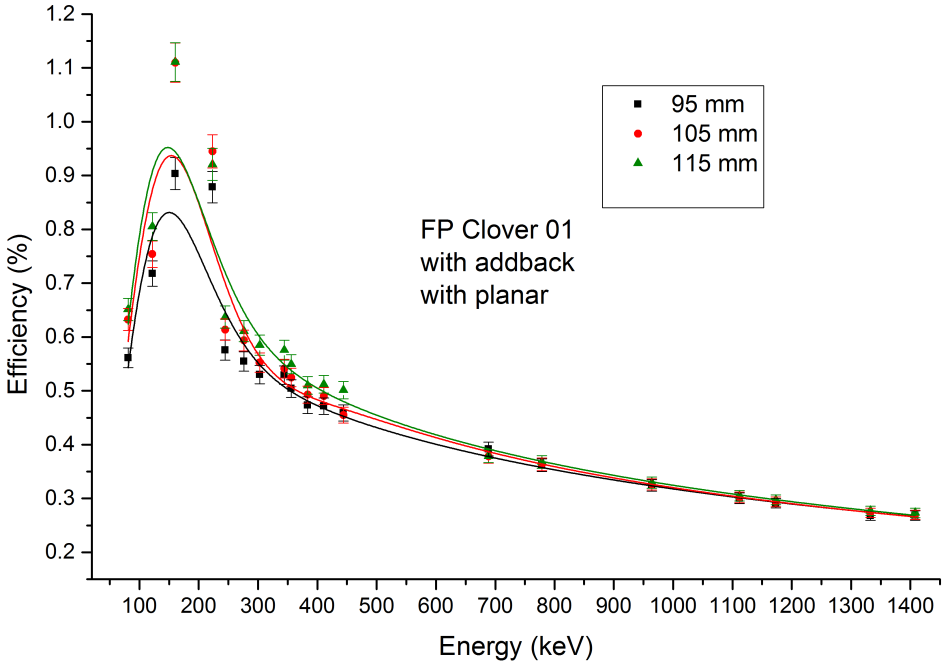

Figure B.4: Efficiency curves for FPClover01 detector, applying add-back code.

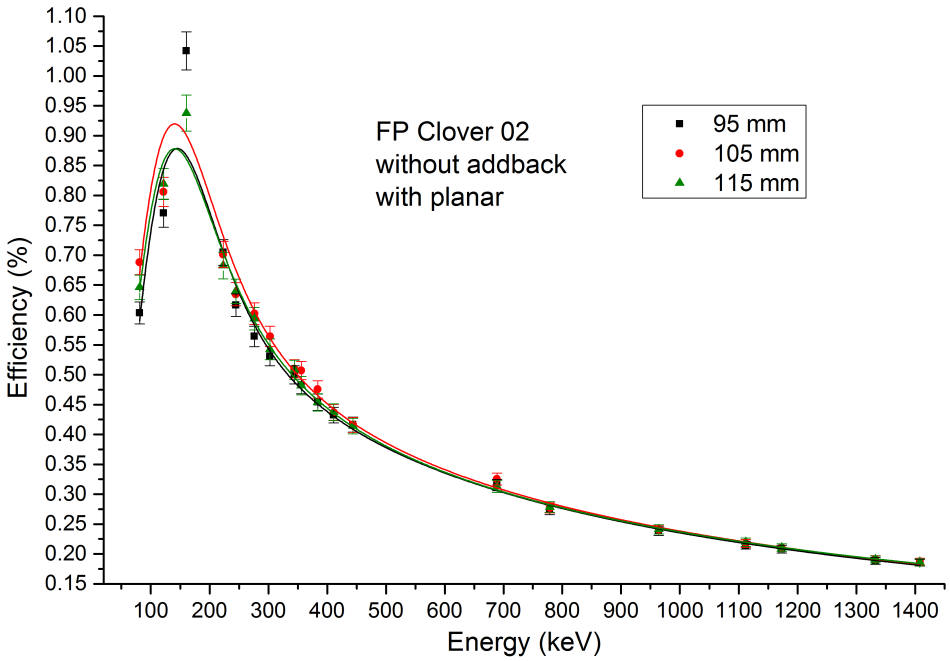

Figure B.5: Efficiency curves for FPClover02 detector, without application add-back code.

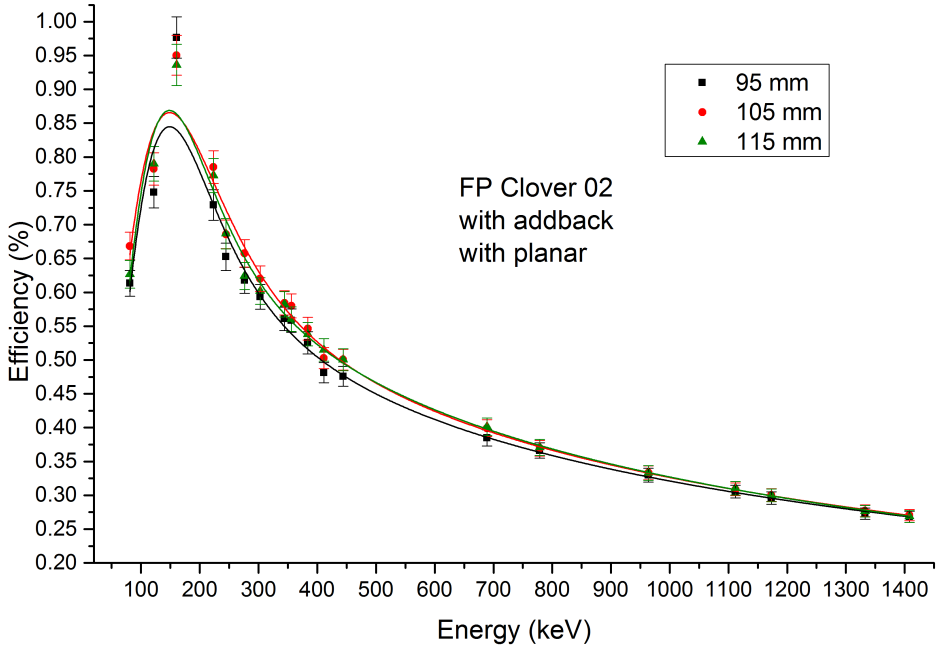

Figure B.6: Efficiency curves for FPClover02 detector, applying add-back code.

Appendix C

Plots for measurement without planar detector

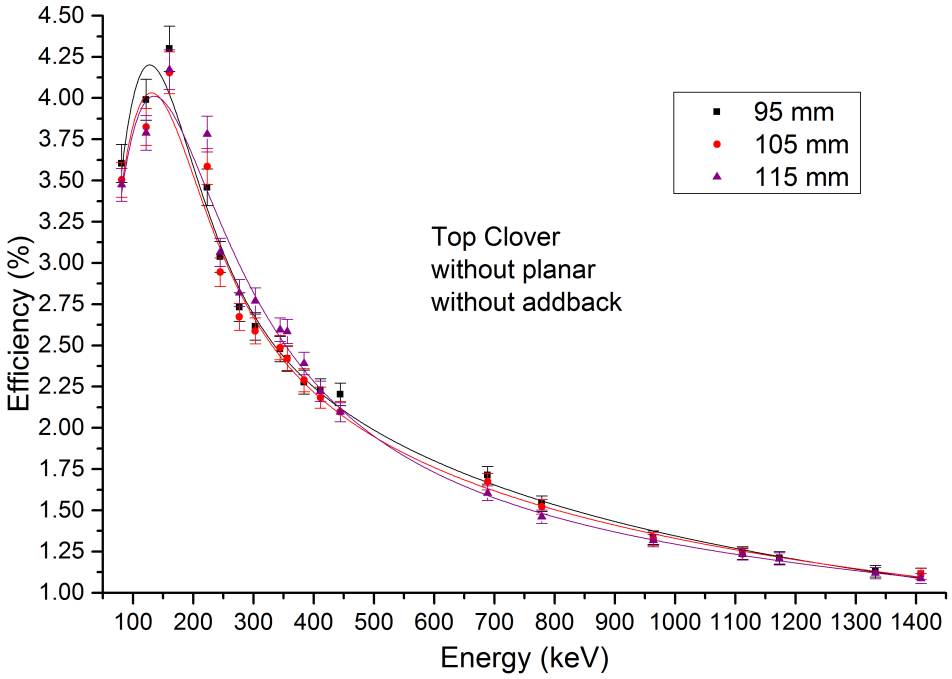

Figure C.1: Efficiency curves for Top Clover detector, without application add-back code.

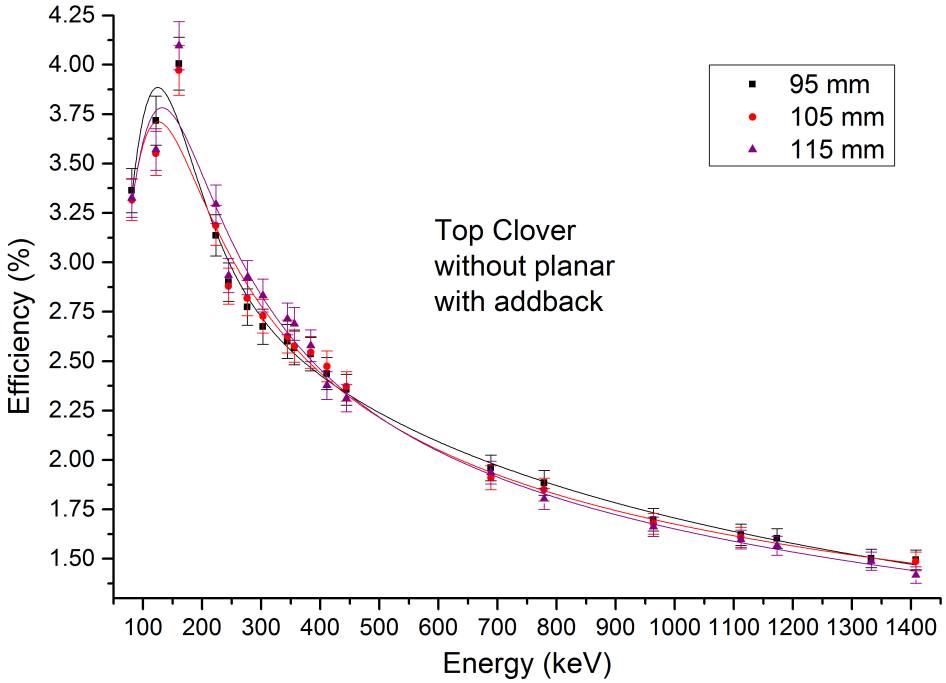

Figure C.2: Efficiency curves for Top Clover detector, applying add-back code.

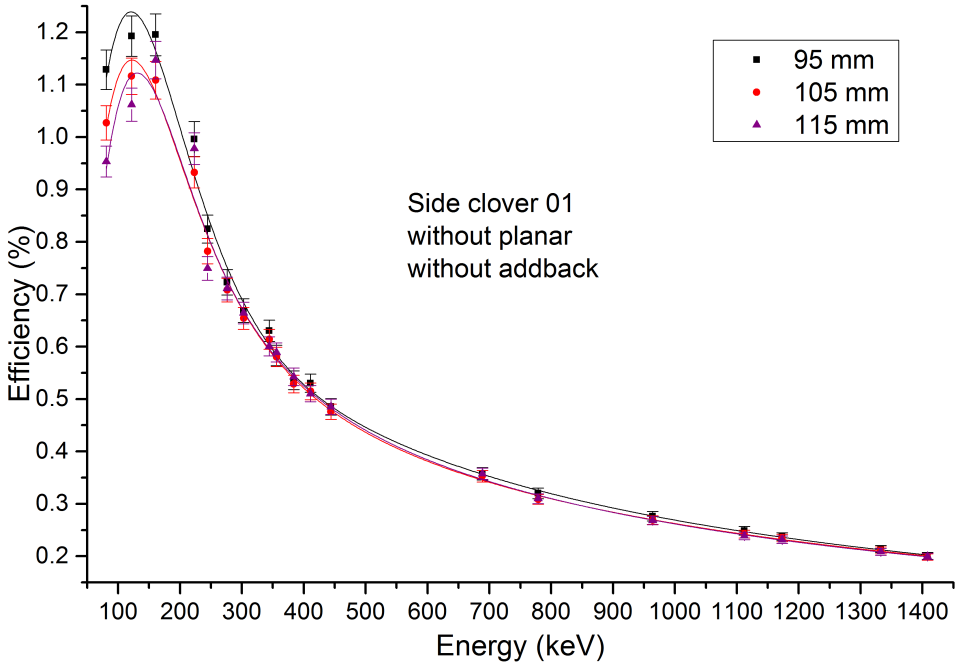

Figure C.3: Efficiency curves for FPClover01 detector, without application add-back code.

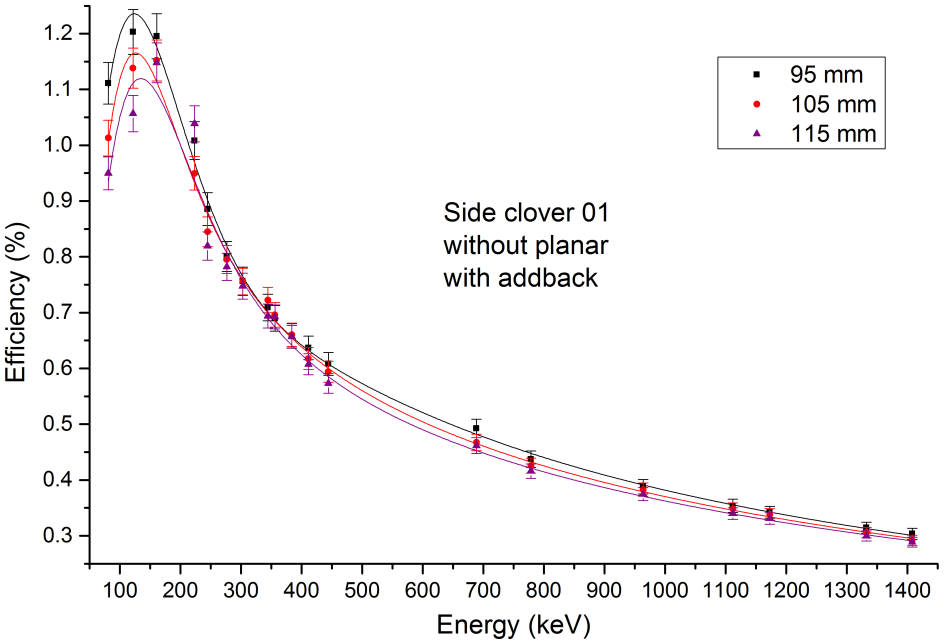

Figure C.4: Efficiency curves for FPClover01 detector, applying add-back code.

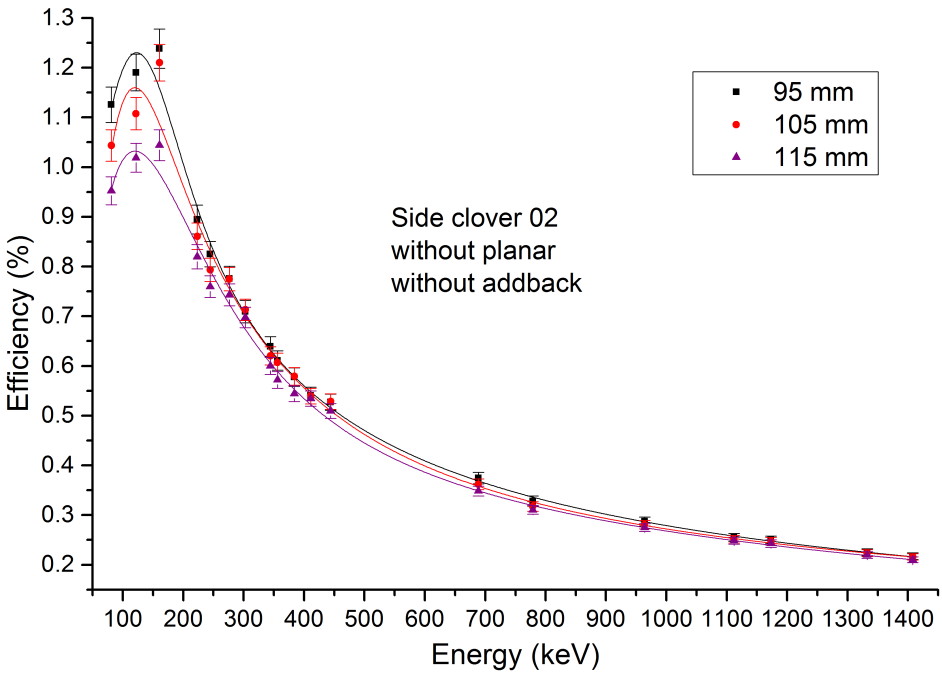

Figure C.5: Efficiency curves for FPClover02 detector, without application add-back code.

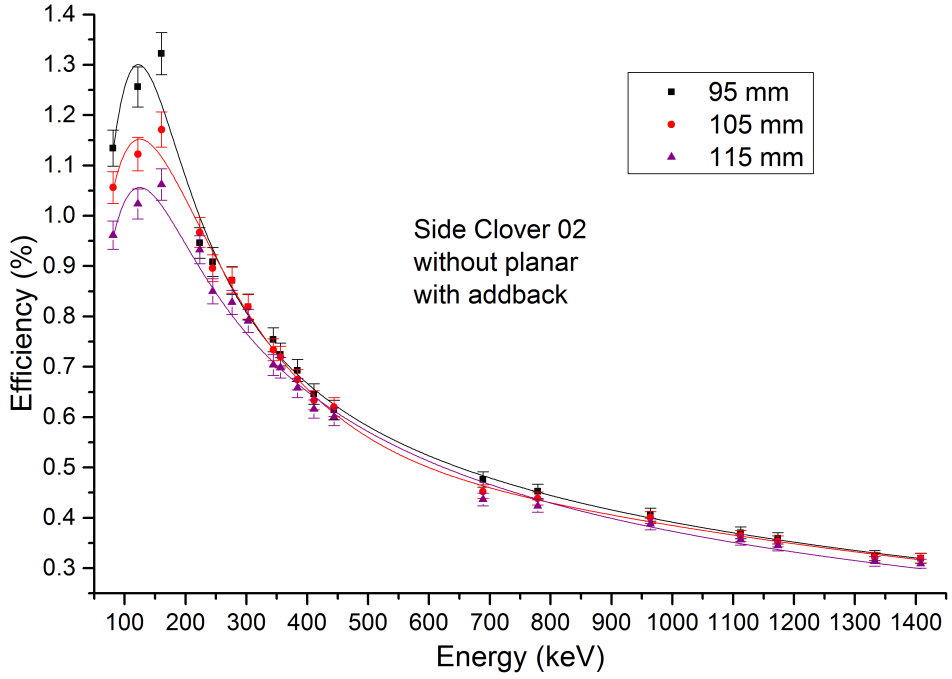

Figure C.6: Efficiency curves for FPClover02 detector, applying add-back code.